https://doi.org/10.5194/egusphere-2026-5435
Preprint. Discussion started: 14 September 2026

Atlantic Meridional Heat Transports from Ocean Reanalyses, Monitored Sections and Heat Budget Constraints

Susanna Winkelbauer[1], Gaël Forget[2], Michael Mayer[1,3], Romain Bourdalle-Badie[4], Andrea Cipollone[5], Leopold Haimberger[1], Keith Haines[6], Satoshi Osafune[7], Yuanyuan Song[3], Andrea Storto[8], Chunxue Yang[8], and Hao Zuo[3]

[1]Department of Meteorology and Geophysics, University of Vienna, Vienna Austria
[2]Department of Earth, Atmospheric and Planetary Sciences, Massachusetts Institute of Technology, Cambridge, United States
[3]European Centre for Medium-Range Weather Forecasts, UK, Germany
[4]Mercator Ocean International, France
[5]CMCC Foundation – Euro-Mediterranean Center on Climate Change, Bologna, Italy
[6]Dept. of Meteorology, University of Reading, and National Centre for Earth Observation, UK
[7]Japan Agency for Earth-Marine Science and Technology (JAMSTEC), Yokosuka, Japan
[8]Institute of Marine Sciences, National Research Council of Italy, Rome, Italy

Correspondence: Susanna Winkelbauer (susanna.winkelbauer@univie.ac.at)

Abstract. Meridional ocean heat transport (MHT) plays a central role in the climate system by redistributing energy across latitudes and influencing global and regional climate variability. While sustained observing systems in the Atlantic, subpolar North Atlantic and Arctic gateways provide valuable observational constraints on Atlantic heat transport, their spatial coverage remains limited and assessing their uncertainties remains challenging. Ocean reanalyses offer a complementary, spatially complete view of the ocean, but their ability to represent Atlantic heat transport across those gateways has so far not been consistently assessed.

Here we evaluate MHT estimates from 17 global ocean reanalyses using in-situ observational transport estimates and complementary heat-budget-derived transport estimates. The assessment covers major observing sections across the Atlantic and Arctic Oceans, including the South Atlantic Meridional Overturning Circulation Basin-wide Array (SAMBA), the RAPID array at 26.5°N, the Overturning in the Subpolar North Atlantic Program (OSNAP), the Greenland-Scotland Ridge (GSR), Davis Strait, Fram Strait and the Barents Sea Opening.

The two sets of estimates generally agree within two sigmas, despite the fact that biases and errors cannot be fully accounted for (whether in mooring-based estimates or in reanalyses). We demonstrate this level of agreement both for the meridional structure and for temporal variability in MHT. Temporal correlations are as high as 0.75–0.8 at RAPID and 0.65–0.75 at the GSR, but significant differences exist in both mean state and variability. Increasing resolution in reanalyses tends to improve agreement with observational estimates when computed from monthly temperature and velocity output. However, for one degree reanalyses it is essential to include the parameterized eddy terms (advective and diffusive) rather than using temperature and velocity output. Accounting for these parameterized contributions removes significant but artificial biases in MHT at this resolution.

https://doi.org/10.5194/egusphere-2026-5435
Preprint. Discussion started: 14 September 2026

The reanalysis ensemble mean shows lower mean heat transport than the mooring based estimates at RAPID and Fram Strait, while showing higher transport through the Barents Sea Opening. Hence there is significant uncertainty in terms of the partitioning of Arctic heat inflow pathways. Heat-budget-derived transport estimates show generally good agreement with the available transport observations across the evaluated sections. The representation of variability depends strongly on region and timescale. At RAPID and the GSR, the considered reanalyses show the highest consistency with observational estimates across seasonal to interannual timescales, whereas OSNAP is the most challenging section. Trend analyses from the reanalysis ensemble indicate a broad reduction of northward Atlantic heat transport across most gateways since the early 1990s, although substantial uncertainties remain prior to the Argo era. At the RAPID latitude (26.5°N), the full reanalysis ensemble indicates 1993–2023 declines of -0.058 ± 0.039 PW decade^{-1} in MHT.

1 Introduction

The redistribution of heat by the global ocean is a fundamental component of Earth's climate system, shaping the exchange of energy between low and high latitudes and influencing regional climate variability and long-term climate change(Trenberth and Caron, 2001; Fasullo and Trenberth, 2008; Forget and Ferreira, 2019). In the Atlantic Ocean, northward heat transport associated with the Atlantic Meridional Overturning Circulation (AMOC) strongly influences air-sea heat exchange, atmospheric circulation, Arctic and European climate, and the storage of excess heat in the ocean (Buckley and Marshall, 2016; Trenberth and Fasullo, 2017; Forget and Ferreira, 2019). Understanding the variability and long-term evolution of Atlantic heat transport is therefore essential for improving our understanding of climate variability and trends, as well as for evaluating climate model simulations and for long-range prediction systems.

Direct observational estimation of ocean heat transport remains limited to a small number of sustained observing systems and hydrographic sections. While these observing systems provide highly valuable constraints on ocean circulation and transport variability, their spatial coverage is necessarily sparse and most records are so far relatively short compared to the timescales of climate variability and trends. Complementary approaches have been developed that combine Argo observations and other spatially resolved observational datasets with models to infer meridional heat transports, providing an alternative to transport estimates from individual observing sections (Forget et al., 2008a, b). Ocean reanalyses (ORAs) have also become increasingly important tools for investigating ocean heat transport variability, as they can provide dynamically consistent and spatially complete estimates of the evolving ocean state over multiple decades. The North Atlantic remains uniquely well suited for evaluating ocean heat transport estimates because it is spanned by multiple sustained observing systems extending from the subtropical Atlantic to the Arctic gateways, such as RAPID (Johns et al., 2011; McCarthy et al., 2015), OSNAP (Lozier et al., 2019), SAMBA (Kersalé et al., 2020) and Arctic gateway monitoring programs (Tsubouchi et al., 2021). Those observational networks enable a systematic assessment of reanalysis-derived heat transports across a wide range of latitudes and circulation regimes. It should be noted, however, that mass transport estimates from sustained observing systems are themselves subject to methodological uncertainties. These arise from assumptions required to close the mass and freshwater transport budgets, including the treatment of unsampled regions, mass conservation constraints, and boundary conditions, as well as the geostrophic

https://doi.org/10.5194/egusphere-2026-5435
Preprint. Discussion started: 14 September 2026

assumption (Stepanov et al., 2016) and differing assumptions regarding exchanges through connecting gateways such as the Bering Strait (McCarthy et al., 2020; Sinha et al., 2018). Heat transport estimates additionally require adequate temperature sampling across the section, which for extended sections relies on complementary observations such as Argo profiles.

At the same time, substantial uncertainties remain in ocean reanalysis estimates of heat transport, arising from differences in model resolution, atmospheric forcing, data assimilation methodologies and representation of key circulation features such as boundary currents, overflows and mesoscale variability. A number of recent studies have evaluated ocean reanalysis heat transports against individual observing systems. Comparisons at the Greenland-Scotland Ridge have shown that most modern reanalyses reproduce the observed variability reasonably well, although systematic differences remain in both mean transports and variability amplitudes (Mayer et al., 2023b). Similar assessments at OSNAP revealed substantially larger discrepancies between reanalyses and observational transport estimates, particularly on interannual timescales (Winkelbauer et al., 2026; Baker et al., 2022). Recent work suggests that some of these discrepancies may however arise from uncertainties in the observational estimates and should not be attributed solely to deficiencies in the reanalyses (Winkelbauer et al., 2026). In the South Atlantic, Baker et al. (2023) found considerable differences between reanalysis-, altimetry- and heat-budget-derived transport estimates at the SAMBA latitude. In the Arctic and Nordic Seas, several studies have documented substantial differences among ocean reanalyses in the representation of gateway transports, water-mass properties and heat exchanges, emphasizing the continued need for systematic evaluation against sustained observations (Uotila et al., 2019; Winkelbauer et al., 2022, 2024b). While these studies provide valuable insights for individual observing systems, a comprehensive assessment of heat transport using a consistent methodology across the full Atlantic observing network is still lacking.

This study is carried out within the framework of the Ocean Decade: Marine Environment Reanalyses Evaluation Project (MER-EP, UNESCO Ocean Decade, 2025), Yang et al. (2026a), which aims to systematically evaluate and intercompare global ocean and marine reanalyses across a broad range of variables, processes and user-oriented applications. MER-EP builds upon earlier coordinated ocean reanalysis intercomparison efforts, most notably the Ocean Reanalyses Intercomparison Project (ORA-IP; Balmaseda et al. (2015)), which demonstrated both the value of multi-reanalysis ensembles and the substantial uncertainties that remain in key aspects of the ocean state estimation. While ORA-IP primarily focused on large-scale physical ocean properties, including ocean heat content, sea level and mixed-layer depth, it also included targeted assessments of circulation and transport diagnostics (Jackson et al., 2019). MER-EP seeks to provide a more systematic evaluation of the most recent marine reanalyses using more process-based use cases spanning ocean physics, sea ice, waves and biogeochemistry.

In addition to direct observational estimates, we also evaluate the reanalyses against heat transport estimates derived from the vertically integrated ocean heat budget (Trenberth et al., 2019; Mayer et al., 2023a). These budget-constrained estimates combine net surface heat fluxes, temporal ocean heat content tendencies and thermodynamic sea ice contributions, thereby providing an observationally constrained estimate of heat transport variability that is derived independently of the circulation fields of the ocean reanalyses themselves. Recent studies have demonstrated the potential of such approaches for estimating large-scale ocean heat transport variability at regional to global scales (Meyssignac et al., 2024; Calafat et al., 2025; Pan et al., 2026). The approach is particularly useful for investigating interannual and longer-term variability, although uncertainties in ocean heat content tendencies remain an important source of uncertainty in the inferred MHT (Meyssignac et al., 2024).

https://doi.org/10.5194/egusphere-2026-5435
Preprint. Discussion started: 14 September 2026

By combining direct observations, energy-budget estimates and a large ensemble of ocean reanalyses (ORAs), this study aims to assess the robustness, consistency and structural uncertainty of Atlantic Ocean heat transport estimates across a wide range of latitudes and timescales. This includes long-term trends, which may be related to changes in the strength of the AMOC (Terhaar et al., 2025).

2 Data and Methods

This section describes the study region, datasets and methods used in this study. Figure 1 provides an overview of the Atlantic study domain and the observational transport sections considered. We first introduce the ORAs along with the indirect heat transport estimates derived from the vertically integrated ocean heat budget, followed by the observation section-based transport estimates.

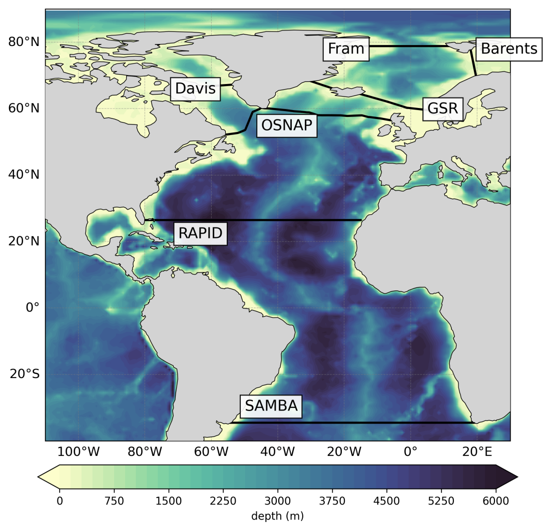

Figure 1. Map of Atlantic bathymetry showing sections and straits where observation based estimates are available.

2.1 Direct Calculation of Transports from Ocean Reanalysis

We analyse a collection of 17 global ORAs from several international forecasting and climate centres (see Table 1 for more details and explanation of acronyms). The ensemble includes products from ECMWF, CMCC, Mercator Ocean, the UK Met Office, MIT, JAMSTEC, the University of Maryland and CNR-ISMAR; spanning horizontal resolutions from 1° to eddy-rich 1/12° configurations. The products assimilate in situ temperature and salinity profiles, satellite sea level anomalies and sea surface temperature observations, while differing substantially in their ocean models, atmospheric forcing, data assimilation schemes, selected insitu and satellite data products and their quality control. The ensemble includes both closely related systems (e.g. the GREP-family products based on NEMO; Desportes et al., 2017; Storto et al., 2019) and methodologically diverse

https://doi.org/10.5194/egusphere-2026-5435
Preprint. Discussion started: 14 September 2026

products, including the ECCO ocean state estimate (Forget et al., 2015; ECCO Consortium et al., 2021b, a) and the SODA (Carton et al., 2018) and ESTOC (Osafune et al., 2015) ocean reanalyses, thereby sampling a broad range of structural uncertainties in ocean model systems. ORAS6-pilot is a pilot version of the ECMWF ocean and sea-ice ensemble reanalysis ORAS6 (**?**). It differs from the final ORAS6 system in several respects, including the observations assimilated and the settings used for sea-level anomaly assimilation. Only the unperturbed member of ORAS6-pilot is used in this study. None of the products assimilate the insitu transport observations used for the evaluation presented here, such as RAPID or OSNAP mooring velocities, and much of the section-specific hydrography is also not assimilated. However, some underlying observational information may overlap with data assimilated by the reanalyses. The use of this large and diverse ensemble allows us to assess the robustness of inferred heat transport variability across the ORAs and to better quantify structural uncertainty than in previous assessments.

Ocean heat transports are calculated from monthly mean velocity and temperature output of the ORAs following equation 1. Monthly output was used because it is the highest temporal resolution consistently available across the full reanalysis ensemble. Daily fields retain sub-monthly covariance terms between velocity and temperature that are not explicitly represented when heat transport is calculated from monthly mean fields. While neglecting these covariance terms may introduce small differences in the estimated heat transport at some latitudes (Valdivieso et al., 2014, , Fig 3), monthly output was considered sufficient enough for the purpose of this study. A comparison using daily and monthly GLORYS12V1 fields (Appendix Fig. A1) shows that differences in the mean transport are largest in parts of the Southern Ocean, near the equator and around 35-40°N, while the temporal variability agrees closely over most latitudes. The largest differences in deseasonalized heat transports occur around 35-40°N and south of approximately 40°S. Throughout this study, we refer to transports across latitude sections as meridional heat transport (MHT) and to transports through ocean gateways or straits, which additionally contain a zonal component, as ocean heat transport (OHT).

$$OHT_{ORA} = c_p \rho \int_{x_l}^{x_r} \int_{z_1(x)}^{z_2(x)} (\theta(x,z) - \theta_{ref}) \boldsymbol{v}(x,z) \cdot \boldsymbol{n} dz dx, \tag{1}$$

where $\boldsymbol{v} \cdot \boldsymbol{n}$ is the velocity component normal to the section, θ the potential temperature, θ_{ref} a reference temperature, ρ the seawater density and c_p the specific heat capacity of seawater. Since many considered sections do not exhibit perfectly closed mass budgets, heat transports depend on the choice of reference temperature (Schauer and Beszczynska-Möller, 2009). In principle, this ambiguity can be reduced by choosing a reference temperature representative of the transport-weighted mean temperature of the flow across each section (Bacon et al., 2015). However, because the present study compares heat transports across a wide range of Atlantic sections and reanalysis products, we adopt the commonly used reference temperature of $\theta_{\text{ref}} = 0°\text{C}$ for all calculations. This ensures a consistent definition of heat transport throughout the analysis, although the absolute values remain reference-temperature dependent (Forget and Ferreira, 2019). Transport calculations are performed on the native model grids using the StraitFlux framework (Winkelbauer et al., 2024a) or using MeshArrays.jl (Forget et al., 2015) to ensure consistency with the underlying model discretization. Transport calculations are generally based on the resolved

https://doi.org/10.5194/egusphere-2026-5435
Preprint. Discussion started: 14 September 2026

Ocean Reanalysis	Resolution	Time Period	Institute	Documentation
ORAS6-pilot, ORAS5	1/4°, 75 layers	1993–2024	European Centre for Medium-Range Weather Forecasts (ECMWF)	Zuo et al. (2019)
CGLORSv8, CGLORSv7	1/4°, 75 layers	1993–2023/2021	Centro Euro-Mediterraneo sui Cambiamenti Climatici (CMCC)	Storto and Masina (2016)
GLORYS4V2, GLORYS2V4	1/4°, 75 layers	1993–2022/2021	Mercator Ocean	Garric and L.Parent (2016)
GloRanV14, GloSIA9-1	1/4°, 75 layers	1993–2021/1994–2020	MetOffice	MacLachlan et al. (2015)
GLORYS12V1	1/12°, 50 layers	1993–2025	Mercator Ocean	Lellouche et al. (2018); Jean-Michel et al. (2021)
ECCO4r6, OCCA2	1°, 50 layers	1992–2025, 1992–2023	Massachusetts Institute of Technology (MIT)	Forget et al. (2015), Forget (2026)
			Jet Propulsion Laboratory (JPL)	ECCO Consortium et al. (2021b, a)
SODAV3.15.2	1/4°, 50 layers	1993–2023	University of Maryland	Carton et al. (2018)
SODAV4.15.2	1/10°, 75 layers	1993–2023	University of Maryland	Chepurin et al. (2025)
CIGAR, CIGAR0.25	1°, 1/4°, 75 layers	1993–2024	National Research Council, Institute of Marine Sciences (CNR-ISMAR)	Storto and Yang (2024)
ESTOCv3a, ESTOCv7a	1°, 46 layers	1993–2014/2022	Japan Agency for Marine Earth Science and Technology (JAMSTEC)	Osafune et al. (2014, 2022)

Table 1. Summary of the ORA products used in this study, including their horizontal and vertical resolution, temporal coverage, producing institution, and reference documentation.

https://doi.org/10.5194/egusphere-2026-5435
Preprint. Discussion started: 14 September 2026

monthly three-dimensional velocity and temperature fields (U, V, T) provided by the reanalyses. For the coarse-resolution ECCO, OCCA and ESTOC products, for which additional diffusive and parameterized eddy-induced (bolus) heat transport components are available, these contributions are included in the total MHT used throughout the analysis. This provides a physically more complete estimate and improves consistency with eddy-permitting and eddy-rich products, where a larger fraction of mesoscale heat transport is explicitly resolved. For CIGAR at $1°$ resolution, these additional components are not available, and MHT is therefore calculated from the resolved velocity and temperature fields only. The sensitivity of coarse-resolution MHT estimates to the inclusion of parameterized transport components is examined in Sect. 3.1.

2.2 Heat Budget-derived

To complement the directly estimated ocean heat transports (OHT), we additionally derive indirect estimates OHT$_{inf}$ based on the vertically integrated ocean heat budget approach described in Mayer et al. (2023a). In this framework, OHT across a latitude or ocean section is inferred from the balance between net air–sea heat fluxes and temporal ocean heat content tendencies integrated over the ocean area enclosed between the section of interest and a reference chokepoint where OHT is either known and/or small, together with the observed heat transport through that reference chokepoint.

$$OHT_{inf} = OHT_{cp} - \int\limits_{S} \left[F_S(x,y) - \rho_0 c_p \frac{\partial}{\partial t} \int\limits_{z_1}^{z_2} (\theta_o(x,y,z) - \theta_{ref}) dz - L_f \rho_i \frac{\partial d_i(x,y)}{\partial t} - R_{Adj} \right] \mathrm{d}S \tag{2}$$

where S is the ocean surface area between the chokepoint section (e.g. Bering Strait) and the section of interest (e.g. RAPID).

Here, F_S denotes the net downward surface heat flux, θ_o the ocean temperature, θ_{ref} a reference temperature, d_i the sea-ice thickness, ρ_0 and ρ_i the densities of seawater and sea ice (set constant to 1026 kgm^{-3} and 928 kgm^{-3} respectively). The terms in brackets represent the area-integrated contributions from net surface heat fluxes, ocean heat content tendencies and sea ice melt energy tendency (the tendency of latent heat of fusion associated with sea ice changes) in S. To ensure global consistency between surface heat fluxes and ocean heat storage, a spatially uniform monthly adjustment R_{Adj} is applied following Trenberth et al. (2019); Mayer et al. (2023a).

This method yields continuous OHT estimates across latitude bands of the Atlantic, the Indo-Pacific, and global oceans, including the major observational sections. For Atlantic estimates, the heat budget is integrated between the latitude of interest and a reference chokepoint section where OHT estimates are available. In contrast, global meridional OHT estimates are obtained from the vertically integrated global ocean heat budget from either North or South Pole without requiring an external chokepoint constraint, as the zonal integration around the globe forms a closed domain. Heat-budget-derived transport estimates are calculated for SAMBA, RAPID, OSNAP and the GSR. Separate estimates are not derived for the individual Arctic gateways, as the comparatively small transports and larger influence of sea-ice energy terms increase the uncertainty of such estimates. In addition, deriving individual transports through Fram Strait and Barents Sea Opening would require assumptions about the partitioning of heat transport among those gateways.

https://doi.org/10.5194/egusphere-2026-5435
Preprint. Discussion started: 14 September 2026

Surface heat fluxes are estimated indirectly from the atmospheric energy budget. This combines net radiation at TOA from the Clouds and the Earth's Radiant Energy System–Energy Balanced and Filled (CERES-EBAF Loeb et al., 2018) and DEEP-C (Liu et al., 2020) datasets, with the divergence of atmospheric energy transports as well as atmospheric energy storage based on the ERA5 (Hersbach et al., 2020), MERRA2 (Gelaro et al., 2017), JRA55 (Kobayashi et al., 2015), and JRA-3Q (KOSAKA et al., 2024) atmospheric reanalyses. Energy budgets from reanalyses are diagnosed following (Mayer et al., 2024). Ocean heat content tendencies are obtained from the IAPv4 (Cheng et al., 2024), RFROM (Lyman and Johnson, 2023) and ORAS5. Sea-ice melt energy tendency is estimated from GIOMAS (Zhang and Rothrock, 2003) and ORAS5. As reference chokepoint transports we use monthly observational transport estimates from Tsubouchi et al. (2024) and Fredriksen et al. (2025) for three boundary configurations: (i) Bering Strait (mean: 1.4 $\pm$ 0.8 TW), (ii) the combined Arctic gateways (Davis Strait, Fram Strait and Barents Sea Opening; mean: 0.14 $\pm$ 0.04 PW), and (iii) Davis Strait together with the Greenland–Scotland Ridge (mean: 0.31 $\pm$ 0.05 PW).

The heat-budget-derived estimates are therefore not generally independent of all datasets used in the ORA evaluation. ORAS5 is furthermore used for ocean heat content and sea-ice melt energy tendencies in some realizations, while the observational chokepoint transports used as boundary constraints are also included among the direct transport estimates evaluated in this study. The data used is summarized in Table 2. Uncertainties are quantified as twice the standard deviation (2σ) across different combinations of atmospheric and oceanic datasets used in the budget calculation.

variable	datasets
Fs inferred	ERA5, JRA55, MERRA2, JRA3Q
OHCT	IAPv4, RFROM, ORAS5
IHCT	GIOMAS, ORAS5
OHT$_{cp}$	Bering , Davis+Fram+BSO, Davis+GSR

Table 2. Datasets and reference chokepoint configurations used for the heat-budget-derived ocean heat transport estimates. The table lists the atmospheric, oceanic and sea-ice datasets, together with the reference chokepoint transports used in the heat-budget integration. Chokepoint transport estimates are taken from Fredriksen et al. (2025) and Tsubouchi et al. (2024).

Similar energy-budget-based approaches have recently been applied by Meyssignac et al. (2024) to infer heat transports between OSNAP and RAPID, and by Calafat et al. (2025) using observational constraints from Argo, satellite altimetry, and gravimetry to derive basin-scale Atlantic heat transport estimates. More recently, Pan et al. (2026) applied a closely related framework to estimate global and basin-scale meridional heat transports from ocean heat content tendencies and surface fluxes, but using a different energy-budget adjustment methodology based on constrained optimization and spatial covariance structures. Together, these studies support the robustness of indirect energy-budget approaches for estimating large-scale ocean heat transport variability.

https://doi.org/10.5194/egusphere-2026-5435
Preprint. Discussion started: 14 September 2026

2.3 In-situ and altimeter based estimates

Neither the direct transport calculations from reanalyses nor the indirect approaches use derived current velocities, which are available only at dedicated sections with sustained observing systems and hydrographic programs in the Atlantic and Arctic Oceans (Fig. 1). These include the RAPID array at 26.5°N in the subtropical North Atlantic (Johns et al., 2011; McCarthy et al., 2015; Moat et al., 2026), the OSNAP observing system in the subpolar North Atlantic (Lozier et al., 2017; Fu et al., 2025), and the SAMBA array at 34.5°S in the South Atlantic (Kersalé et al., 2020, 2021). In the Arctic and Nordic Seas, we additionally use transport estimates from the Greenland-Scotland Ridge (GSR) (Tsubouchi et al., 2021; Mayer et al., 2023b), as well as Davis Strait, Fram Strait and the Barents Sea Opening based on inverse-model estimates constrained by extensive moored observations (Fredriksen et al., 2025; Tsubouchi et al., 2024). Uncertainties associated with these observational transport estimates are taken from the original data products where available. For RAPID, we follow the uncertainty estimates of Johns et al. (2011, 2023), as also adopted by Meyssignac et al. (2024), accounting for both statistical uncertainty associated with temporal variability and potential measurement and methodological biases. For SAMBA, we adopt the published total uncertainty from Kersalé et al. (2021). For OSNAP and the GSR, uncertainties are taken directly from the corresponding observational products. For the Arctic gateway estimates, uncertainty is estimated from the spread across the available observational transport reconstructions (Fredriksen et al., 2025; Tsubouchi et al., 2024). For the 12-month running-mean time series, monthly observational uncertainties are propagated assuming independent errors. Mean observational transports and the associated uncertainties used throughout this study are summarized in Appendix Table A1.

Additionally, comparisons are made with meridional heat transport estimates derived from the AX07 (30°N) and AX18 (35°S) repeat XBT transects. These products are based on repeated trans-basin expendable bathythermograph (XBT) observations combined with satellite altimetry and atmospheric reanalysis data and provide independent estimates of Atlantic heat transport variability (Baringer and Garzoli, 2007; Garzoli et al., 2013). Given the relatively short duration of the SAMBA record, we additionally consider the altimeter-based meridional heat transport estimates of Dong et al. (2021), which extend the South Atlantic transport record back to 1993 and are derived by combining satellite altimetry and in situ observations with atmospheric reanalysis winds. While these estimates provide valuable additional temporal coverage, they are not fully independent of the ORAs evaluated here. Comparisons with the Dong et al. (2021) product should therefore be interpreted as complementary to, rather than replacing, the direct validation against the SAMBA observations.

These observational products provide the best available constraints on Atlantic heat transport, although they differ in methodology and degree of independence from the ORAs evaluated here. The mooring-based observing systems derive basin-scale transports by combining measurements from moorings, hydrographic observations and, in some cases, additional observing platforms such as gliders, with interpolation and inverse-model techniques. Consequently, uncertainties may arise not only from measurement errors but also from observational gaps and the methods used to reconstruct spatially continuous transport fields (Winkelbauer et al., 2026). In contrast, the XBT- and altimeter-based products share some input data with many ORAs and therefore should not be seen as fully independent.

https://doi.org/10.5194/egusphere-2026-5435
Preprint. Discussion started: 14 September 2026

Strait	Period	Reference
RAPID	2004/04 - 2023/12	Moat et al. (2026)
OSNAP	2014/08 - 2022/07	Fu et al. (2025)
GSR	1993/01 - 2021/07	Tsubouchi et al. (2021)
Fram, Barents, Davis	2004/10 - 2024/07	Fredriksen et al. (2025)
SAMBA	2013/09 - 2017/07	Kersalé et al. (2020, 2021)
Altimeter-based at 34.5°S, 30°S, 25°S, 20°S, 26.5°N	1993–2025	Dong et al. (2021)
XBT at 35°S, 30°N	2002–2019, 1994–2024	Baringer and Garzoli (2007), Garzoli et al. (2013)

Table 3. Sections with current observation systems used for the evaluation of ocean heat transport (OHT) across the Atlantic and Arctic Oceans. The table lists the observing sections, the periods used in the analysis, and the corresponding references. Comparisons with reanalysis products are performed over the maximum available overlap between each observational record and the reanalysis time series. Mean observational transport estimates and their associated uncertainties are provided in Appendix Table A1.

2.4 Methodological considerations

2.4.1 AMOC calculation at sections

In addition to meridional heat transport, we evaluate the Atlantic Meridional Overturning Circulation (AMOC) strength at the RAPID section (26.5°N). The overturning streamfunction is calculated in depth coordinates from the monthly mean meridional velocity fields by vertically integrating the zonally integrated transport from the ocean bottom upward,

$$\Psi(z) = \int_{z_b}^{z_0}\int_{x_l}^{x_r} v(x,z')\,\mathrm{d}x\,\mathrm{d}z', \tag{3}$$

where v is the meridional velocity normal to the section, x_l and x_r denote the western and eastern boundaries of the section, z_b is the local ocean bottom, and z' is depth. Positive values correspond to northward transport. The AMOC strength is then defined as the maximum of the overturning streamfunction.

2.4.2 Mass flux constraints at sections

For OSNAP, a mass-flux constraint is applied and transports are calculated directly from the model velocity fields. This correction is needed to match the methodology of the observational product (Lozier et al., 2019). Specifically, a southward throughflow of 1.6 Sv is prescribed across OSNAP West, representing an observational estimate of the long-term mean export through Davis Strait, and is compensated by an equal northward transport across OSNAP East to satisfy the basin-wide mass budget. As this adjustment can affect the barotropic variability across the section, its influence was assessed in a sensitivity test (not

https://doi.org/10.5194/egusphere-2026-5435
Preprint. Discussion started: 14 September 2026

shown). The adjustment affects the mean transport and, to a lesser extent, the seasonal cycle, while its influence on deseasonalized and low-frequency variability is small.

The constraint is implemented in StraitFlux through a barotropic velocity correction. A spatially uniform compensation velocity is added over the entire wet cross-sectional area,

$$v_{\mathrm{corr}} = \frac{Q_{\mathrm{target}} - Q_{\mathrm{raw}}}{A}, \tag{4}$$

where Q_{raw} is the volume transport calculated directly from the model velocities, Q_{target} is the prescribed target volume transport and A is the total oceanic cross-sectional area. The corrected transport is then obtained by adding v_{corr} to the normal velocity at every wet grid cell. This correction is applied only for OSNAP in order to follow the definition of the observational transport estimate and ensure a consistent comparison between reanalyses and observations.

2.5 Uncertainty quantification

Uncertainties in the reanalysis-derived heat transports are quantified as twice the inter-product standard deviation ($\pm 2\sigma$) across the reanalysis ensemble, which provides a measure of the uncertainty associated with differences in model formulation, resolution, atmospheric forcing and data assimilation. Uncertainty in the heat-budget-derived estimates is similarly quantified from the spread across the different combinations of atmospheric energy budget, ocean heat content, and sea ice datasets described in Sect. 2.2.

Linear trends are estimated separately for each reanalysis product using ordinary least-squares regression. The uncertainty of the ensemble-mean trend combines the spread among the individual reanalysis trends with the regression uncertainty of the individual trend estimates. Because monthly transport time series exhibit serial correlation, the regression uncertainty is adjusted using an effective sample size based on the lag-one autocorrelation (Santer et al., 2000) of the regression residuals before being combined with the inter-product spread.

To facilitate comparisons across observing sections with different uncertainty ranges, biases are also expressed as standardized biases,

$$z = \frac{OHT_{ORAs} - OHT_{obs}}{\sqrt{\sigma_{obs}^2 + \sigma_{ORAs}^2}}, \tag{5}$$

where OHT_{ORAs} and OHT_{obs} denote the mean reanalysis and observational heat transports, respectively, σ_{obs} is the uncertainty provided for the observational estimate, and σ_{ORAs} is the inter-reanalysis spread. Positive (negative) values indicate overestimation (underestimation) relative to the observations.

https://doi.org/10.5194/egusphere-2026-5435
Preprint. Discussion started: 14 September 2026

3 Results

3.1 Mean Heat Transport

Figure 2 shows the climatological mean meridional heat transport (MHT) as a function of latitude for the global and Atlantic Oceans derived from the ocean reanalyses, and from the indirect energy-budget estimates. Mean transports are calculated over the full available period of each product (see Table 1). Most reanalyses reproduce the large-scale structure of the global ocean heat transport, characterized by southward transports in the Southern Hemisphere and northward transports in the Northern Hemisphere, with maxima in the subtropical oceans. The inferred energy-budget estimate provides the primary observationally constrained reference for the global ocean and exhibits a comparatively smooth latitudinal structure with peak transports of approximately 1.8 PW in the Northern Hemisphere and -1.2 PW in the Southern Hemisphere.

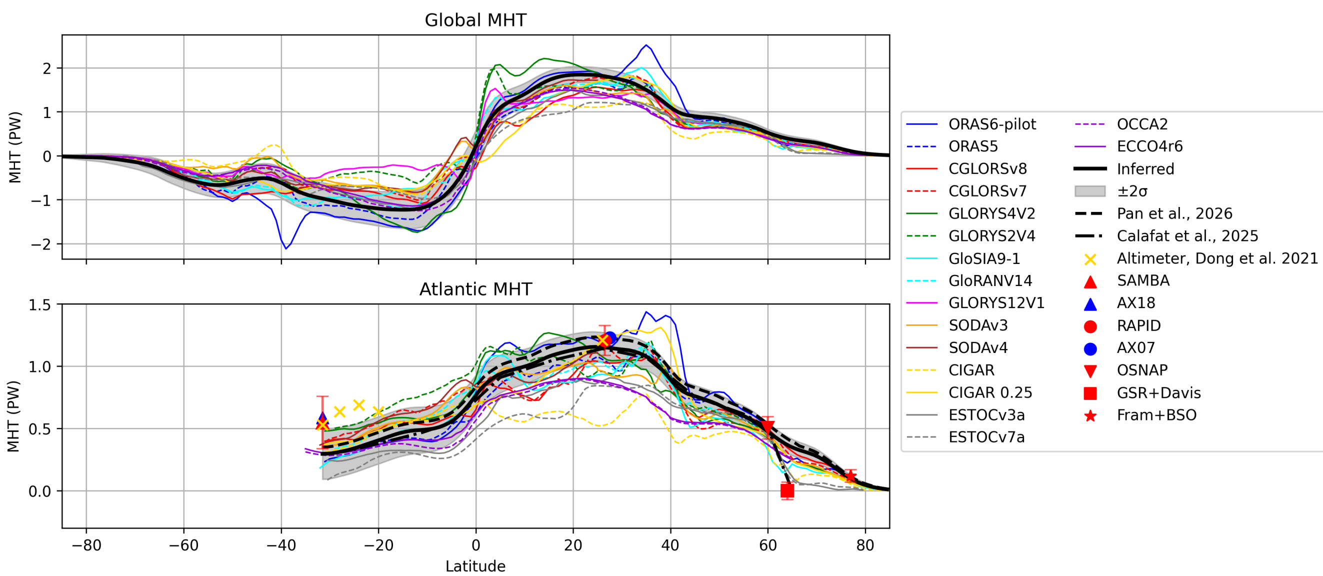

Figure 2. Mean meridional heat transport (MHT) as a function of latitude for the (a) global ocean and (b) Atlantic Ocean. Mean transports are computed over the available period of each product (Table 1). Units are PW. ORAs are compared to inferred estimates (black lines, grey shading indicates the $\pm 2\sigma$ spread), direct observational estimates from hydrographic sections (red and blue symbols) and altimetry-based estimates from Dong et al. (2021) (gold symbols).

Substantial spread exists between individual reanalyses, particularly in the Southern Ocean and at mid-to-high latitudes. While the inter-product spread is larger among the 1/4° and finer-resolution systems (Appendix Fig. A2), this group also contains more products and the difference in spread should therefore not be interpreted as a resolution-dependent effect. In contrast, more systematic biases are evident among the coarse-resolution (1°) products. The resolution-group comparison in Appendix Fig. A2 indicates a clearer low bias in the 1° ensemble across much of the Northern Hemisphere, whereas in the Southern Hemisphere the spread is larger among the 1/4° and finer-resolution products, with several individual reanalysis exhibiting

https://doi.org/10.5194/egusphere-2026-5435
Preprint. Discussion started: 14 September 2026

substantial deviations from the inferred estimate. ORAS6-pilot exhibits pronounced localized extrema around 35–40° in both hemispheres, which are related to the sea-level anomaly assimilation scheme (de Boisséson et al., 2026). Pronounced extrema around approximately 40–50°S are also evident in CIGAR, the only coarse-resolution product for which heat transport is calculated solely from the resolved velocity and temperature fields because additional parameterized transport components are not available. For the other coarse-resolution products, the available diffusive and parameterized eddy-induced heat transport components are included in the total heat transport shown in Fig. 2.

The importance of these additional transport components is illustrated in Fig. 3 for ECCO and ESTOCv7a. In both reanalyses, the transport derived from advective velocity and temperature fields alone exhibits pronounced spurious extrema near 40–50°S, while the inclusion of diffusive and parameterized eddy-induced (bolus) contributions, in particular those associated with Gent–McWilliams-type parameterizations, results in a much smoother and more physically consistent large-scale transport structure and brings the estimates closer to the inferred energy-budget estimate. This demonstrates that transports calculated only from advective components can exhibit artificial spatial variability and biases in coarse-resolution products. Where available, parameterized transport components should therefore be included when evaluating or using MHT from such products. In contrast, the impact of these components is considerably smaller in eddy-permitting and eddy-rich 1/4° and 1/12° products, where mesoscale transports are more explicitly resolved (not shown), although their full contribution requires sufficiently high-frequency velocity and temperature fields to capture transient covariance terms (Valdivieso et al., 2014).

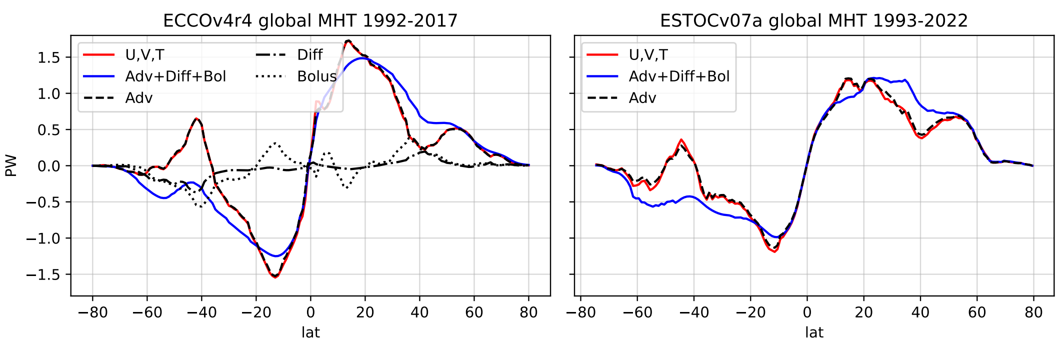

Figure 3. Decomposition of the global meridional heat transport (MHT) into advective, diffusive, and bolus components for (a) ECCO4r4 and (b) ESTOCv7a. The red curve shows the transport computed from monthly mean velocity and temperature fields (U, V, T), while the blue curve includes the additional diffusive and parameterized (bolus) contributions. Units are PW.

For the Atlantic Ocean and Arctic (Fig. 2b), additional constraints are available from direct observational estimates at SAMBA, RAPID, OSNAP, the GSR, Arctic gateways and two XBT sections. Further, altimeter-based estimates from Dong et al. (2021) are also considered. Most ORAs reproduce the observed meridional structure of Atlantic heat transport, including the northward transport throughout the basin and the subtropical maximum near 25°N. However, many products systematically underestimate heat transports compared to observational and inferred estimates, particularly in the subtropical and subpolar North Atlantic. This low bias is most pronounced in coarse-resolution calculations that use monthly temperature and velocity

https://doi.org/10.5194/egusphere-2026-5435
Preprint. Discussion started: 14 September 2026

fields (Appendix Fig. A2). Including the diffusive and bolus transport components significantly reduces artificial biases but not entirely. Quarter degree systems tend to agree more closely with observational estimates, but still often show a low bias.

Figure 4 summarizes the comparison between observational, reanalysis-based and inferred mean heat transport estimates at the major observational sections. Heat-budget-derived estimates are available for SAMBA, RAPID, OSNAP and the GSR, where they agree closely with the corresponding observational estimates and overlap within the reported uncertainties. The ensemble-mean reanalysis estimate also reproduces the observed large-scale transport structure reasonably well, but tends to underestimate transports at several sections. This low bias is most pronounced at the SAMBA and RAPID arrays. At the SAMBA latitude, where the comparison is made against the longer altimetry-based estimate rather than the shorter mooring-derived record, the ensemble-mean reanalysis estimate (0.35±0.18 PW) and the inferred estimate (0.41±0.19 PW) are both lower than the altimetry-based estimate (0.53±0.21 PW). However, these differences remain within the relatively large uncertainty ranges. At the RAPID array at 26.5°N, the ensemble-mean reanalysis estimate (0.91±0.16 PW) falls noticeably below both the observational estimate (1.21±0.12 PW) and the inferred estimate (1.18±0.09 PW), representing the largest systematic low bias among the major observation sections. Part of this apparent low bias may, however, reflect methodological differences between the directly calculated reanalysis transports and the observational estimate. Stepanov et al. (2016) showed that applying RAPID-like geostrophic assumptions to model fields can yield substantially higher MHT than direct calculations from the model velocity field, primarily due to differences in the representation of upper-ocean western boundary circulation.

A particularly interesting behaviour is found at the Arctic gateways. Most ORAs underestimate the observed heat transport through Fram Strait while simultaneously overestimating the transport entering the Barents Sea Opening. Although these biases can be substantial at the individual sections, they partly compensate when both gateways are considered together, resulting in a considerably better agreement with observational estimates of the total heat transport entering the Arctic Ocean. This suggests that differences among reanalyses are associated not only with the total magnitude of northward heat transport, but also with its partitioning between the two Arctic inflow pathways.

Mean MHT values at all sections and for all ORAs are given in Table A1. The standardized biases shown in Fig. 5 provide a complementary view of these differences by accounting for the combined uncertainty of the observational estimates and the reanalysis spread. Consistent with Fig. 4, most reanalyses show negative standardized biases at RAPID, Davis Strait, Fram Strait, SAMBA, OSNAP and the GSR, indicating a tendency to underestimate heat transport relative to the observational reference. Positive biases are mainly confined to the Barents Sea Opening. In contrast to heat transport, volume transport biases (Fig. A3 and Tab. A2) are less systematic across products. Neither the magnitude nor the sign of the biases at Fram Strait and the Barents Sea Opening is consistent across the ensemble. The stronger and more coherent biases found in heat transport therefore cannot be explained by volume transport errors alone, but likely also reflect differences in water-mass properties and possibly heat transport components that are not fully captured by the monthly advective estimates, including high-frequency, eddy induced and diffusive transports.

In Fig. 5, reanalyses are ordered according to their mean absolute standardized bias across all sections. The two ESTOC versions exhibit the largest overall biases, with predominantly negative biases across the evaluated sections. CIGAR also shows comparatively large biases, most notably at RAPID, but is the only coarse-resolution product for which parameterized eddy-

https://doi.org/10.5194/egusphere-2026-5435
Preprint. Discussion started: 14 September 2026

induced and diffusive heat transport components are not available. ECCO4r6 and OCCA2, on the other hand, show smaller overall biases despite their similarly coarse (1°) resolution, with standardized biases at most individual sections comparable to those of many higher-resolution products, although regional differences remain, such as the positive Barents Sea bias in OCCA2. Overall, most eddy-permitting systems (∼1/4° resolution) tend to show smaller standardized biases, but considerable differences remain among individual products and sections. Notably, the highest-resolution products (1/10°-1/12°) do not systematically outperform the best-performing 1/4° systems, suggesting that increased horizontal resolution alone does not guarantee improved representation of large-scale heat transports.

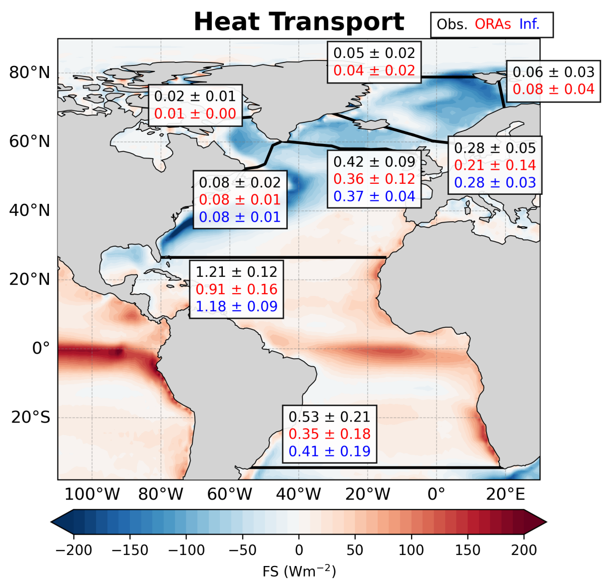

Figure 4. Surface net energy fluxes (colour shading; positive downward) and associated meridional heat transports across key Atlantic sections. Values derived from observational estimates (black), the reanalysis (ORAs) ensemble mean (red), and heat-budget-based inferred estimates (blue) are shown for each section. Observational estimates are taken from the products listed in Table 3, except at the SAMBA latitude, where comparison is made against the altimetry-based estimate of Dong et al. (2021) owing to the relatively short duration of the direct SAMBA observational record. Uncertainties for the reanalysis and inferred ensemble estimates indicate $\pm 2\sigma$ ensemble spread.

3.2 Temporal Variability

While substantial differences exist in the mean transports, agreement in temporal variability is generally reasonable at the majority of straits. Figure 6 shows that most reanalyses reproduce a considerable fraction of the observed low-frequency (12-month running mean) variability at the major observing sections despite the mean-state biases discussed above. This behaviour is reflected in the Taylor-diagram analysis (Fig. 7), where many products exhibit moderate to high correlations with the observations while maintaining variability amplitudes comparable to those observed.

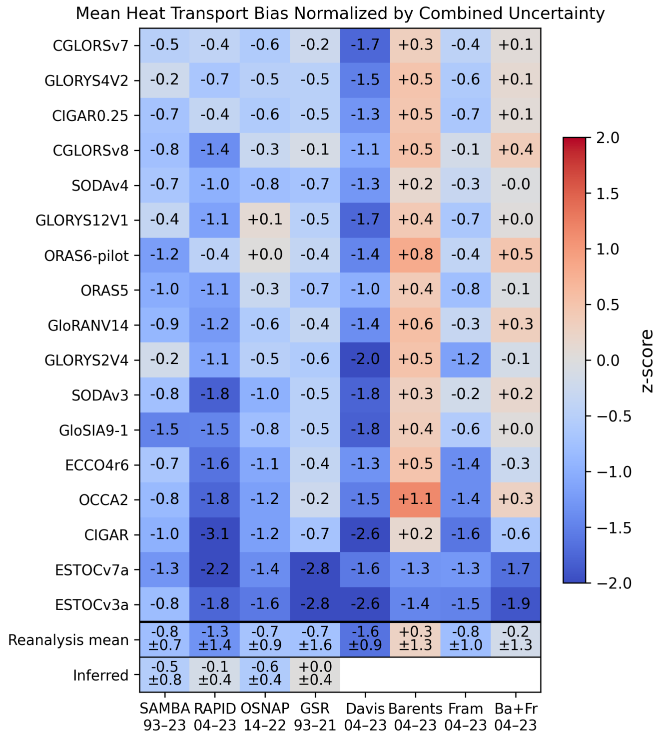

Figure 5. Mean heat transport biases relative to observations expressed as standardized biases (z-scores). Biases are normalized by the combined observational uncertainty and inter-reanalysis spread at each observing section. Positive values indicate overestimation and negative values indicate underestimation relative to observations. An absolute standardized bias $|z| \leq 1$ indicates agreement with the observational estimate within the combined 1-σ uncertainty. Rows are ordered according to the mean absolute standardized bias across all sections. The bottom row shows the heat-budget-derived estimate OHT_{inf} with its 2-σ spread. The last column shows the combined transport through the Barents Sea Opening and Fram Strait. Dates below the section names indicate the averaging period used for the comparison. For ORAs that do not cover the full observational period, means were computed over the available overlapping period only. Observational estimates are taken from the products listed in Table 3, except at the SAMBA latitude, where the comparison is made against the altimetry-based estimate.

The strongest agreement is found at RAPID (26.5°N), where most ORAs cluster around correlations of approximately 0.7–0.9 and normalised variability amplitudes close to 1. The major multi-year fluctuations observed by RAPID are reproduced by the majority of products, indicating that subtropical Atlantic heat transport variability is captured consistently across a wide range of ocean state estimates. An exception is SODAv4, which exhibits substantially poorer agreement than the remainder of the ensemble. The heat-budget-derived estimates generally occupy similar regions of Taylor space as the reanalysis ensemble.

At the SAMBA section, products exhibit substantially weaker agreement on interannual timescales compared to RAPID. The mooring-derived SAMBA observations show considerably larger variability than most ORAs, whereas the longer altimetry-based estimate exhibits variability amplitudes that are more comparable to the reanalysis ensemble. Because of its substantially longer temporal coverage, the altimetry-based (not-independent) product is used as the observational benchmark in the

https://doi.org/10.5194/egusphere-2026-5435
Preprint. Discussion started: 14 September 2026

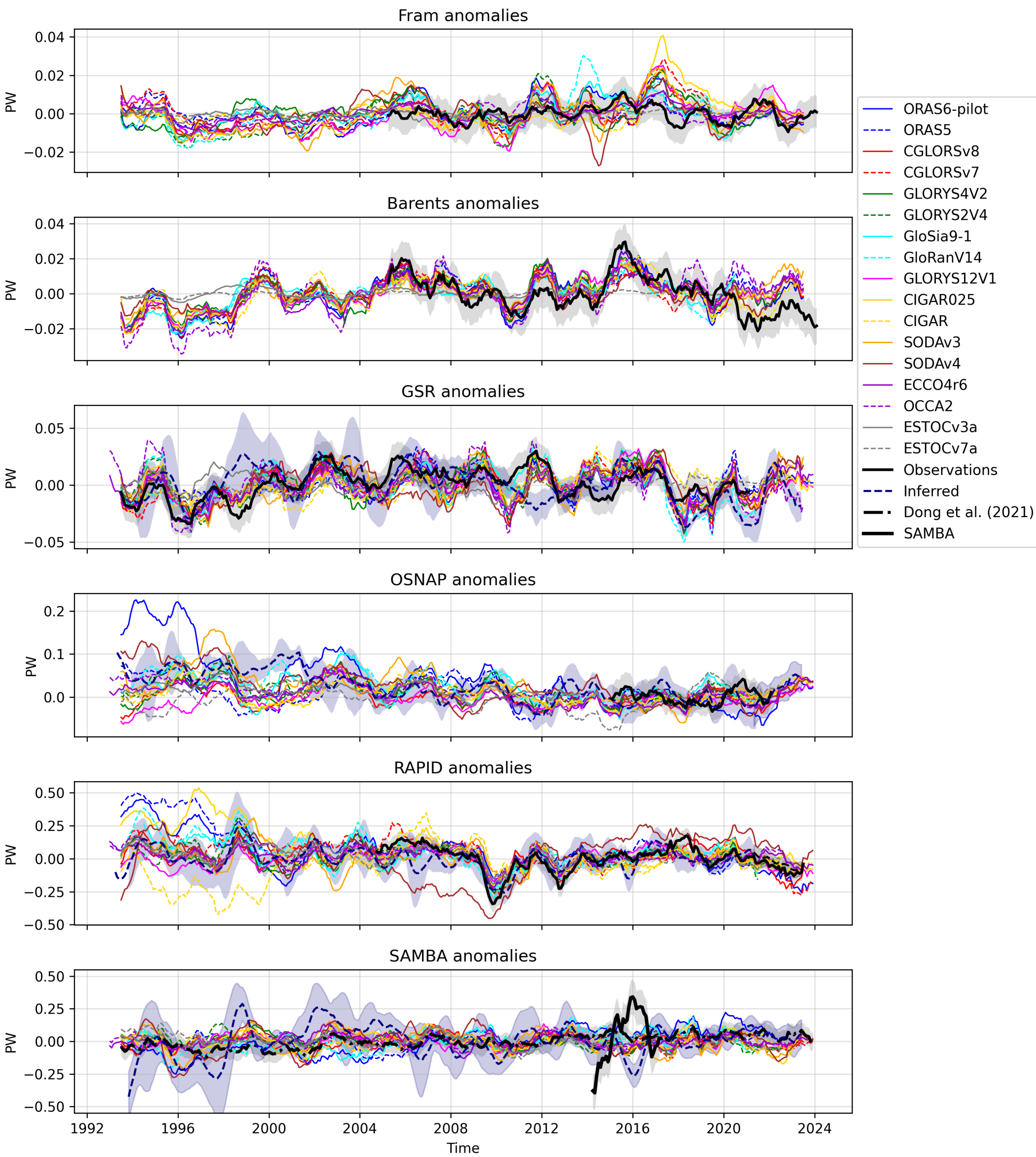

Figure 6. Monthly heat transport anomalies across the SAMBA, RAPID, OSNAP, Greenland–Scotland Ridge (GSR), Fram Strait and Barents Sea sections from observations and ORAs. Anomalies are shown as 12-month running means relative to the temporal mean of each product over the observational period. Black solid lines indicate observations, while colored lines show individual reanalyses. Black dashed lines denote inferred estimates where available, with shading indicating the associated 2σ uncertainty.

correlation analyses. Relative to this benchmark, most reanalyses broadly reproduce the timing of several of the observed anomalies and multiple products show moderate correlations on interannual timescales. The inferred heat-budget estimates display substantially larger variability, with amplitudes that are closer to those observed by the direct SAMBA array than to

https://doi.org/10.5194/egusphere-2026-5435
Preprint. Discussion started: 14 September 2026

the altimetry-based estimate. This enhanced variability however is only weakly correlated with either observational product. Similar behavior was reported by Baker et al. (2023), who showed that heat-budget-derived transport estimates at the SAMBA latitude contain substantial variability that is largely uncorrelated with direct transport observations. The comparatively poor performance of the inferred estimates at SAMBA may partly reflect increasing uncertainty when the heat-budget approach is integrated over large areas towards regions of smaller OHT. Analysis of the individual budget terms indicates that both the surface heat fluxes and the observed ocean heat content tendency contribute substantially to this variability (not shown). The amplitude of the variability of inferred OHT is also somewhat reduced after approximately 2005, consistent with improved observational constraints following the widespread deployment of the Argo observing system.

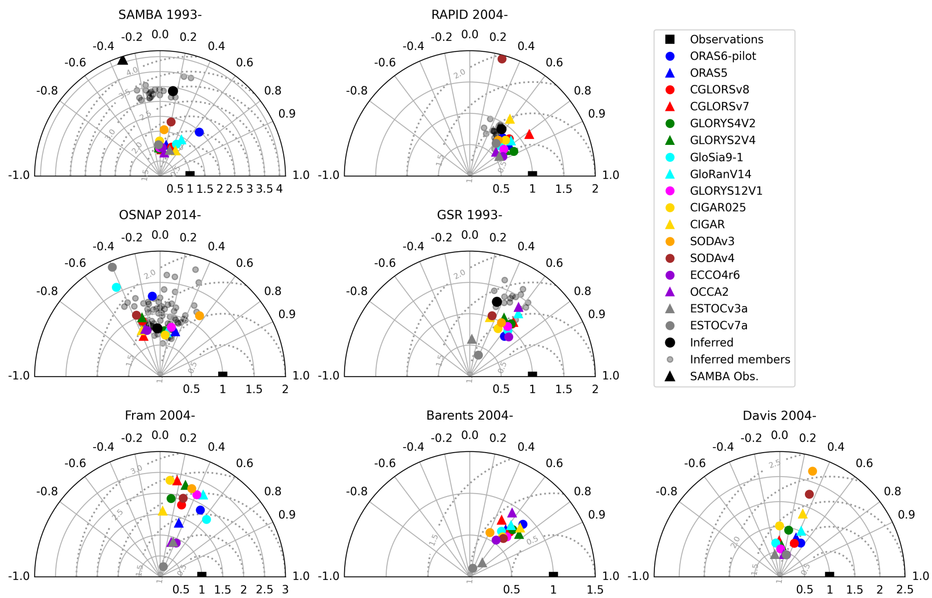

Figure 7. Taylor diagrams comparing low-frequency heat transport variability in ORAs against observations for the SAMBA, RAPID, OSNAP, Greenland–Scotland Ridge (GSR), Fram Strait, Davis Strait and Barents Sea sections. Statistics are computed from 12-month running mean anomalies. Radial distance indicates the standard deviation normalized by observations, angular position indicates the correlation coefficient, and grey contours show centered root-mean-square differences against the available observational estimates. Black symbols represent inferred estimates and inferred-member ensembles for SAMBA, RAPID, OSNAP and the GSR.

The Greenland–Scotland Ridge also exhibits relatively good agreement, with correlations typically around 0.5–0.7 and variability amplitudes close to those observed. As already shown by Mayer et al. (2023b) reanalyses generally reproduce both the timing and magnitude of the observed low-frequency variability, resulting in a comparatively compact distribution in Taylor space, with an exception of the ESTOCv3a reanalysis, which shows no correlations with the observed values.

https://doi.org/10.5194/egusphere-2026-5435
Preprint. Discussion started: 14 September 2026

At Fram Strait and the Barents Sea Opening, correlations are generally lower than at RAPID and the Greenland–Scotland Ridge, and larger differences exist in the simulated variability amplitudes. At Fram Strait, several products substantially overestimate variability, whereas ECCO4 and the two ESTOC versions exhibit weaker variability than observed. The spread among products is reflected in the larger range of Taylor statistics at this section. At the Barents Sea Opening, the reanalysis ensemble is more tightly clustered, although ESTOC products again show reduced variability compared with the observations. The weakest agreement is found at OSNAP. Correlations are generally low and both ORAs and heat-budget-derived estimates differ substantially from the observed record. Inspection of the time series indicates that much of the discrepancy is associated with a small number of pronounced transport anomalies, particularly during 2015 and 2020, when strong peaks in overturning MHT observed in OSNAP East are not reproduced by either the ORAs or the inferred estimates (Winkelbauer et al., 2026).

3.2.1 Seasonal Cycles

The seasonal cycle of heat transport is generally reproduced qualitatively by the reanalysis ensemble, although notable differences in phase, amplitude, and mean transport remain among products (Fig. 8). SAMBA exhibits a pronounced seasonal cycle, with maximum heat transport during austral winter and a minimum during spring to early summer. Most ORAs reproduce the timing of this cycle, but sometimes show reduced seasonality and mean transport as compared with the observational estimates. The direct SAMBA observations exhibit a somewhat different seasonal cycle from both the reanalyses and the longer altimeter-based reconstruction of Dong et al. (2021) with a strong peak in late summer. Given the comparatively short observational record however, it is difficult to assess whether these differences reflect robust climatological features or sampling variability. At RAPID, both observations and reanalyses exhibit a minimum heat transport during late winter and early spring and a maximum during summer, with most products reproducing the observed timing and amplitude of the annual cycle despite a tendency to underestimate the mean transport. OSNAP, in contrast, displays a comparatively weak seasonal cycle and larger differences between products and observations. The weak seasonal variability of the combined OSNAP transport largely reflects the contribution from OSNAP West, whereas the eastern branch exhibits a more pronounced seasonal cycle similar to that at the Greenland–Scotland Ridge, with the summer minimum occurring approximately one month later (not shown). At the Greenland–Scotland Ridge (GSR), the observed seasonal cycle is characterized by a minimum during late spring to early summer and a maximum during autumn and early winter. While the broad structure of this cycle is captured by most ORAs, many products exhibit a delayed seasonal minimum and a weaker autumn increase compared to the observations. Farther north, Fram Strait shows a similar seasonal evolution as GSR, with minimum transports during summer and maximum transports in autumn and early winter, although most reanalyses underestimate the mean transport and tend to delay the transition from the summer minimum to the autumn recovery. The Barents Sea Opening exhibits one of the most consistently represented seasonal cycles in terms of its overall shape. Most ORAs show somewhat higher mean transports and seasonal amplitudes than the central observational estimate, although the majority remain within the observational uncertainty range. A slight offset in the timing of the seasonal minima is also evident. Finally, Davis Strait exhibits only a weak seasonal signal and a large relative spread among reanalyses, making robust evaluation more challenging.

https://doi.org/10.5194/egusphere-2026-5435
Preprint. Discussion started: 14 September 2026

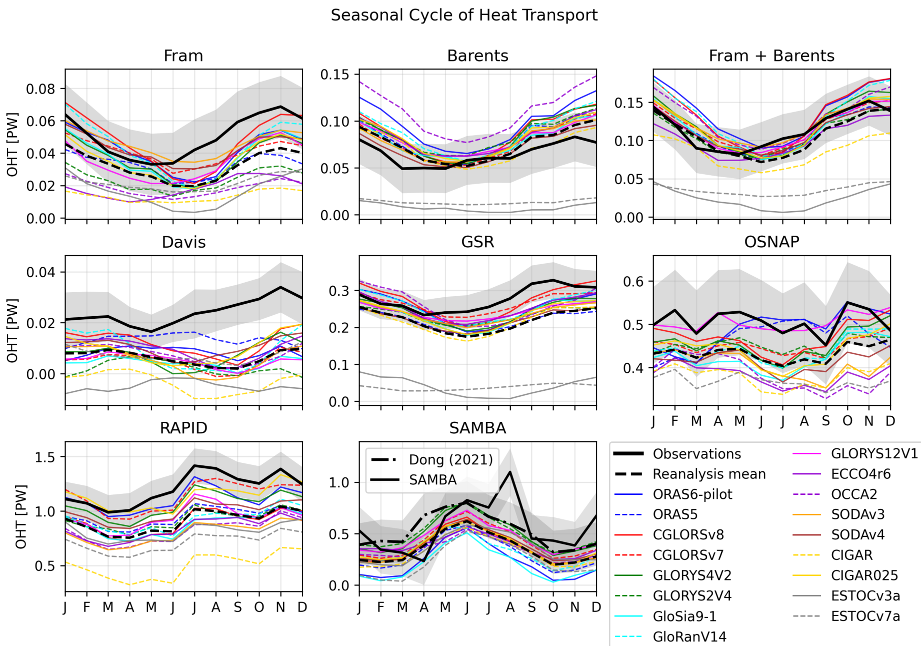

Figure 8. Mean seasonal cycle of heat transport at the SAMBA, RAPID, OSNAP, GSR, Davis, Fram and Barents observing sections. Monthly climatologies were calculated over the maximum overlapping period between each reanalysis and the corresponding observational record. Colored lines show individual ORAs, the dashed black line indicates the reanalysis ensemble mean, and the solid black line shows the observations.

Fig. 9 summarizes heat-transport correlations between the observations and individual reanalyses across timescales, while the correlations for each product are provided in Appendix Fig. A5. RAPID exhibits consistently high skill across all timescales, with median correlations of about 0.85 for the seasonal cycle and remaining near 0.75-0.8 for monthly anomalies and 12-month running means. GSR also shows robust skill across all timescales, although with lower median correlations of approximately 0.65-0.75 and comparatively small inter-reanalysis spread. SAMBA, Fram and Barents all show strong seasonal-cycle agreement, with median correlations around 0.8–0.95, but their skill decreases substantially for monthly and low-frequency anomalies. This decrease is especially pronounced at SAMBA, where correlations drop from over 0.9 for the seasonal cycle to below about 0.2 for 12-month running means. Fram and Barents exhibit a similar, although less pronounced, reduction in skill with increasing timescale. Davis Strait behaves differently from the other sections, with weak seasonal-cycle agreement and somewhat higher median correlations at monthly to annual timescales. These correlations are, however, generally not statistically significant and vary substantially across products. In contrast, OSNAP emerges as the most challenging section, with correlations decreasing from modest seasonal-cycle agreement to near-zero or negative values for annual and low-frequency variability. This behaviour suggests substantial disagreement between ORAs and observations on interannual timescales and may reflect both limitations in the reanalyses and uncertainties in the observational estimate itself (Winkelbauer et al., 2026).

https://doi.org/10.5194/egusphere-2026-5435
Preprint. Discussion started: 14 September 2026

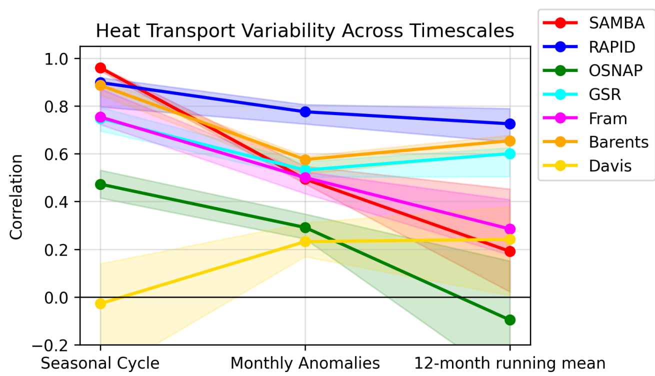

Figure 9. Representation of heat transport variability across timescales in Atlantic and Arctic observing sections. Correlations between observed and reanalysis-derived heat transports are shown for the seasonal cycle, deseasonalized monthly anomalies and 12-month running mean anomalies. Lines indicate the median correlation across all ORAs, while shaded envelopes denote the interquartile range (25th–75th percentile). Correlations were calculated over the maximum overlapping period between each reanalysis and observational record.

3.3 Trends

Figure 10 summarizes linear trends in Atlantic meridional heat transport (MHT) derived from the reanalysis ensemble for the periods 1993–2023 and 2004–2023. For both periods, the ensemble-mean trend indicates a broad reduction of northward heat transport throughout much of the Atlantic basin. The strongest negative trends occur in the tropical and subtropical North Atlantic, with weaker trends at higher latitudes. Normalizing the trends by the climatological mean MHT (not shown) does not substantially alter the overall spatial pattern of MHT changes. However, the normalized decline, expressed as a percentage of the mean MHT per decade, becomes more pronounced in the subpolar North Atlantic, reflecting the smaller climatological mean transport in this region.

The spatial pattern of the ensemble-mean trend is broadly similar for the two periods, although trend amplitudes are generally larger at higher latitudes when the analysis is extended back to 1993. This difference is associated with stronger declines during the pre-Argo observing era, when the ocean observing system was scarcer.

The uncertainty associated with these trends arises from two sources: disagreement among reanalysis products and uncertainty in the estimation of individual linear trends. Appendix Fig. A6 shows that the relative importance of these contributions varies with latitude and analysis period. Trend estimation uncertainty is generally larger for the shorter 2004–2023 period because fewer years are available to constrain the linear trend, whereas inter-product spread tends to increase when the analysis is extended into the pre-Argo era. Despite the larger spread in the earlier period, most reanalyses indicate negative MHT trends over the North Atlantic, suggesting that the basin-scale weakening of northward Atlantic heat transport is a robust feature across a wide range of ocean state estimates, although its precise magnitude remains uncertain. The largest overall uncertainties occur in the tropical Atlantic and around 35–40°N, where trends are largest and reanalysis products show substantial disagreement in both the magnitude and the sign of long-term trends.

https://doi.org/10.5194/egusphere-2026-5435
Preprint. Discussion started: 14 September 2026

Inspection of individual products (Appendix Fig. A7) indicates that part of this spread originates from a small number of ORAs exhibiting strong low-frequency variability and long-term trends prior to the Argo period. In particular, ORAS5, ORAS6-pilot and CIGAR0.25 contribute disproportionately to the ensemble spread before the mid-2000s. In the case of ORAS5, the non-stationary behaviour has been attributed to difficulties of the assimilation system to realistically constrain OHT in the early period with little sub-surface observational data (Tietsche et al., 2020).

Two products were excluded from the trend analysis because of limitations in temporal coverage or known issues in their long-term behaviour. SODA4 was omitted because preliminary evaluation revealed unrealistic low-frequency variability and low correlations when compared with the broader reanalysis ensemble and available observations. ESTOCv3a was excluded because its record ends in 2014. GloSIA9-1 terminates before the end of the analysis period (2023), but was retained because it provides a complementary estimate over a substantial fraction of the study period. The resulting ensemble therefore represents a compromise between maximizing the number of independent estimates and maintaining temporal consistency across the analysis period.

Figure 10b shows trends calculated from an ensemble of heat-budget-derived estimates (see Appendix Fig. A8 for the individual realizations). Similar to the reanalysis ensemble, the inferred estimates indicate predominantly negative MHT trends throughout much of the Atlantic. However, the ensemble-mean trends are generally not statistically significant. This is consistent with Mayer et al. (2023a), who similarly found that heat-budget-derived Atlantic OHT trends were generally associated with substantial uncertainty and were statistically significant only over limited latitude ranges. Appendix Fig. A8 demonstrates that both the magnitude and significance of the inferred trends depend on the atmospheric reanalysis, the applied energy-budget adjustment method and the choice of integration boundary, although all realizations consistently indicate a reduction of northward heat transport across much of the basin. The inferred trends are generally associated with smaller uncertainties when integrating from the Greenland–Scotland Ridge and Davis Strait than from Bering Strait. This is consistent with the smaller integration domain and the reduced contribution of Arctic heat storage and sea-ice processes to the integrated heat budget. The sensitivity to the adjustment method highlights another important source of uncertainty in heat-budget-derived transport estimates. The globally uniform adjustment applied following Trenberth et al. (2019); Mayer et al. (2023a) is designed to ensure consistency between globally integrated surface heat fluxes and observed ocean heat uptake. However, alternative approaches distribute the required adjustment regionally according to estimated spatial uncertainty structures or regional energy imbalances rather than uniformly across the global ocean (e.g. Liu et al., 2020; Liu, 2026; Yang et al., 2026b). In the present analysis, these regional adjustment methods generally produce somewhat larger negative MHT trends than the globally uniform adjustment, with some individual estimates becoming statistically significant, while the overall conclusion of a basin-wide reduction in northward heat transport remains unchanged.

At the RAPID latitude (26.5°N, Fig. 11), the ORA ensemble-mean trend over 2004–2023 is in close agreement with the observed RAPID trend. Both estimates indicate a decline of approximately 0.03 PW decade^{-1}, with overlapping uncertainty ranges, although the ORA ensemble-mean trend over this period is not statistically significant. This agreement is notable given that none of the reanalysis products assimilates the RAPID velocity observations directly. Extending the analysis back to 1993 yields a stronger and statistically significant negative ensemble-mean trend of -0.058 ± 0.039 PW decade^{-1}. The inter-product

https://doi.org/10.5194/egusphere-2026-5435
Preprint. Discussion started: 14 September 2026

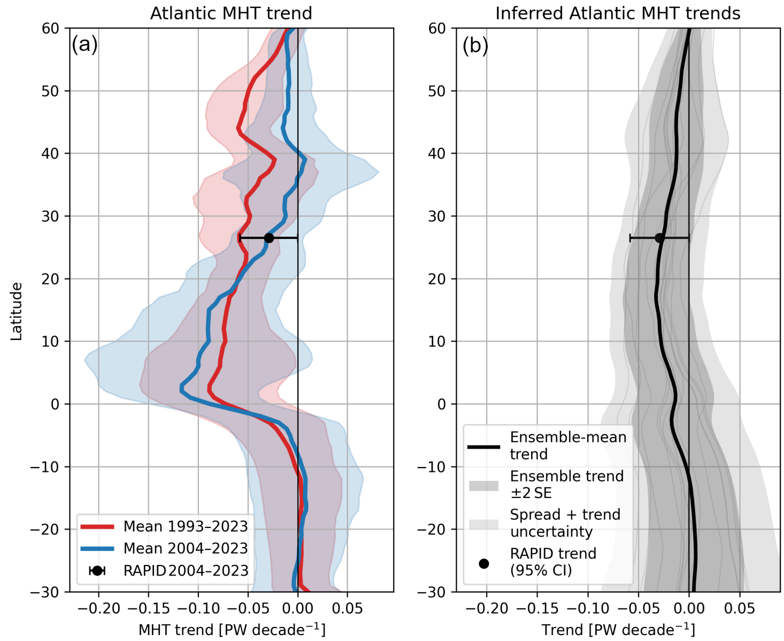

Figure 10. *a)* Linear trends in Atlantic MHT estimated from an ensemble of ORAs over the periods 1993–2023 (red) and 2004–2023 (blue). Solid lines show the ensemble-mean trends, the shaded envelopes indicate the combined uncertainty, calculated as the quadratic sum of the inter-product ensemble spread and the trend-estimation uncertainty ($\pm 2\mathrm{SE}_{\mathrm{AR1}}$), following a similar approach as used by Mayer et al. (2022). *b)* MHT trends inferred from surface heat fluxes using an ensemble of estimates based on different atmospheric reanalyses, integration boundaries, and adjustment methods (Table A4). The black line shows the ensemble-mean inferred trend. The dark grey shading indicates the uncertainty of the ensemble-mean trend ($\pm 2\mathrm{SE}_{\mathrm{AR1}}$), while the light grey shading shows the combined uncertainty obtained from the quadratic sum of the trend uncertainty and the spread among the inferred estimates. The black marker shows the RAPID 26.5°N MHT trend for 2004–2023, with horizontal error bars indicating the 95% confidence interval of the trend estimate. Negative values indicate a reduction in northward heat transport. Trends are expressed in PW decade^{-1}.

spread is also substantially larger during the pre-Argo period. Much of this enhanced spread originates from a small number of ORAs exhibiting pronounced anomalies during the 1990s, which may in part reflect initialization and spin-up effects. Consistent with the discussion above, ORAS5 exhibits a particularly strong shift during this period (Tietsche et al., 2020). Excluding ORAS5 reduces the 1993–2023 ensemble-mean trend to -0.050 ± 0.039 PW decade^{-1} and excluding both ORAS5 and CIGAR025, the two products with the strongest negative trends, yields -0.045 ± 0.037 PW decade^{-1}. Both estimates remain statistically significant, indicating that the negative ensemble-mean trend is not solely driven by these outliers. All 14 ORAs exhibit negative trends over the 1993–2023 period, of which eight are statistically significant, although their magnitudes vary considerably among products (Table A3). For several reanalyses, the decline is strongest during the earlier part of the record and weaker after approximately 2010, with indications of a renewed decrease in MHT during the most recent years.

https://doi.org/10.5194/egusphere-2026-5435
Preprint. Discussion started: 14 September 2026

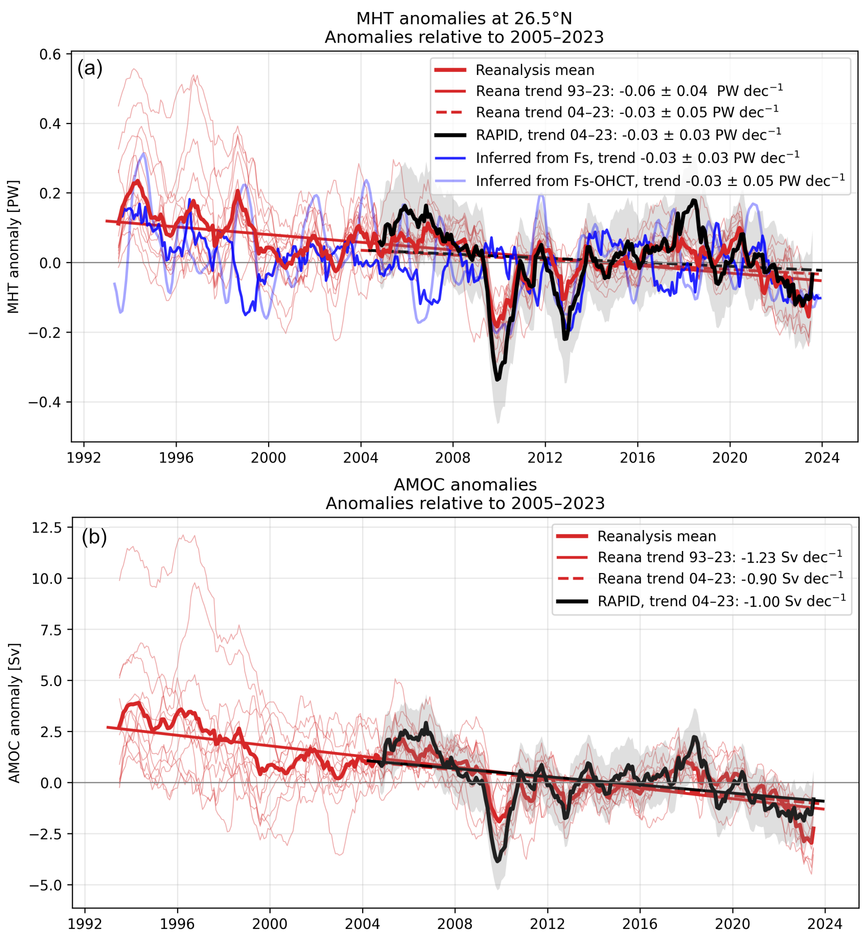

Figure 11. MHT and AMOC anomalies at 26.5°N. *a)* MHT anomalies. *b)* AMOC anomalies. Thin red curves show individual reanalysis products and the thick red curve denotes the ensemble mean. Thick black curves show RAPID observations. The blue curve in the upper panel shows the inferred MHT estimate, calculated as the mean over ERA5, JRA3Q and MERRA2. the light blue curve shows the inferred MHT estimate in combination with IAPv4. All anomalies are referenced to the 2005–2023 mean, except for the inferred estimate, which is referenced to its available period (2005–2021). Solid red lines indicate linear trends calculated from the reanalysis ensemble mean over 1993–2023, and dashed red lines show trends over the RAPID period (2004–2023). The dashed black line shows the RAPID trend over 2004–2023. Displayed anomalies are shown as 12-month running means, while trend estimates are calculated from the unsmoothed anomaly time series.

A complementary perspective is provided by the heat-budget-derived estimates at the RAPID latitude. Figure 11 shows the ensemble-mean inferred MHT anomaly together with the corresponding linear trends obtained using only the surface heat flux term (F_s; dark blue) and in combination with the observed ocean heat content tendency ($OHCT$) from IAPv4 (light blue). Including the observed ocean heat content tendency does not substantially alter the inferred long-term trend, but increases

https://doi.org/10.5194/egusphere-2026-5435
Preprint. Discussion started: 14 September 2026

the temporal variability of the inferred transport estimates and consequently the uncertainty of the trend estimate, consistent with previous studies identifying ocean heat content variability as a major source of uncertainty in heat-budget-derived MHT estimates (Mayer et al., 2023a; Terhaar et al., 2025). Table A4 summarizes the trends obtained for all individual heat-budget realizations. While all inferred realizations indicate negative MHT trends over 1993–2023, most individual realizations, as well as the ensemble-mean inferred trend (-0.03 ± 0.03 PW decade^{-1}), are not statistically significant. Statistically significant declines are obtained primarily for realizations using the adjustment method proposed by Yang et al. (2026b); Liu (2026), whereas trends based on the globally uniform adjustment generally remain absent within uncertainty bounds.

A broadly similar picture emerges for the AMOC (Fig. 11b). The ensemble-mean AMOC time series exhibits a long-term decline that is consistent with the RAPID observations over the 2004–2023 period, although its significance is still debated in literature (Volkov et al., 2024). Extending the analysis back to 1993 yields a stronger ensemble-mean negative trend of -1.23 ± 0.57 Sv decade^{-1}, accompanied by considerably larger inter-product spread during the earlier part of the record. Excluding ORAS5 reduces the ensemble-mean trend to -1.01 ± 0.56 Sv decade^{-1}, while excluding both ORAS5 and CIGAR025 yields -0.87 ± 0.54 Sv decade^{-1}. These estimates overlap within their uncertainty ranges, indicating that the magnitude of the ensemble-mean trend is sensitive to the inclusion of individual products, but that its negative sign is not determined by the two products with the strongest declines. All 14 reanalyses show negative AMOC trends over 1993–2023, of which 12 are statistically significant. Taken together, the reanalyses therefore consistently indicate a weakening of the Atlantic overturning circulation over this period, although its precise magnitude remains uncertain. Figure 12 further demonstrates that both the mean state and long-term trends in Atlantic MHT are closely related to the corresponding AMOC characteristics across the reanalysis ensemble. While products with a stronger mean AMOC generally exhibit larger mean heat transports ($R = 0.83$), the relationship is even tighter for the long-term trends ($R = 0.95$), indicating that differences in simulated MHT trends are closely linked to differences in the strength of the AMOC decline. This suggests that changes in the gyre component of MHT shows relatively little trend - a hypothesis that could be tested using reanalyses.

The larger uncertainty associated with the pre-Argo period (with an approximately 65% larger inter-product spread in 12-month-smoothed MHT anomalies during 1993–2004 than during 2005–2023) is consistent with the evolution of the global ocean observing system. Prior to the widespread deployment of Argo profiling floats, subsurface temperature and salinity observations were substantially sparser and less homogeneous in space and time, particularly outside major shipping routes. Ocean reanalyses and state estimates therefore rely more strongly on model dynamics and data-assimilation properties such as error covariances, resulting in greater structural differences among products. Biases will accumulate freely during the period before Argo, and their magnitude depend on the quality of the free running model and spin up phase used to initialize reanalyses. Users should be aware that this issue is particularly sensitive when sequential data assimilation is used – when Argo assimilation starts it can erase accumulated biases rapidly and induce artificial jumps in MHT and AMOC (Fig. 11).

Nevertheless, the agreement between the RAPID observations and the reanalysis ensemble during their overlapping period provides additional confidence in the observed decline in subtropical Atlantic poleward heat transport during the well-observed Argo era, while the magnitude of the longer-term decline extending into the pre-Argo period remains more uncertain.

https://doi.org/10.5194/egusphere-2026-5435
Preprint. Discussion started: 14 September 2026

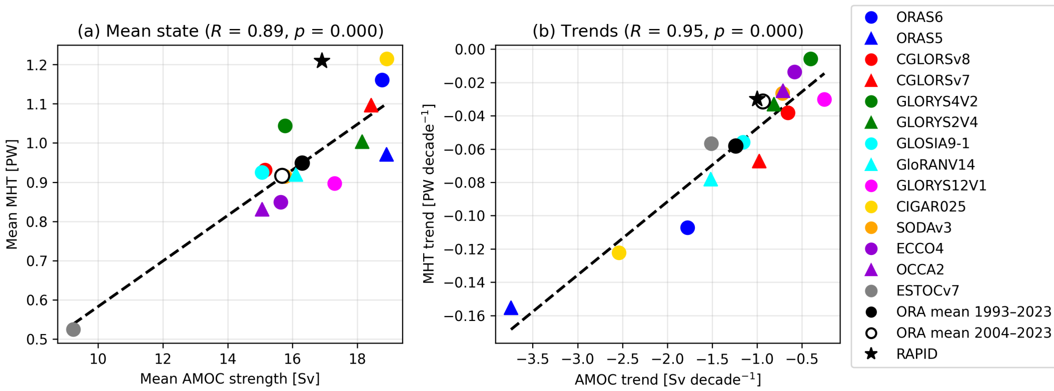

Figure 12. Relationship between Atlantic meridional overturning circulation (AMOC) strength and Atlantic meridional heat transport (MHT) across the ORAs at 26.5N. (a) Mean AMOC strength versus mean MHT for 1993–2023. (b) Linear AMOC trends versus MHT trends over 1993–2023. Colored symbols denote the individual reanalysis products, while the filled black circle indicates the reanalysis ensemble mean for 1993–2023. The open black circle shows the ensemble-mean trend over 2004–2023 and the black star denotes the RAPID observational estimate.

4 Conclusions

This study evaluates Atlantic and Arctic Ocean heat transport in a large ensemble of global ORAs using direct observations and heat-budget-derived estimates. By combining sustained observing systems at SAMBA, RAPID, OSNAP, the Greenland–Scotland Ridge, Davis Strait, Fram Strait and the Barents Sea Opening with energy-budget constraints, we assess the mean state, temporal variability and trends of heat transport across a wide range of latitudes and timescales.

Overall, reanalyses and observational estimates agree on the large-scale structure of Atlantic meridional heat transport, including northward heat transport throughout the Atlantic basin with a subtropical maximum near 25°N. However, substantial differences remain in the magnitude of transports, with most ORAs underestimating heat transports at major Atlantic and Arctic Straits relative to the observational and heat-budget-derived estimates. However, part of the apparent low bias may reflect methodological differences between direct model transport calculations and the observational estimates, for example geostrophic assumptions (Forget, 2010; Stepanov et al., 2016).

Resolution is an important factor controlling the quality of reanalysis heat transport estimates. Coarse-resolution products show the largest standardized biases and can exhibit pronounced artificial extrema in global heat transport when only the resolved advective transport is available. The artificial nature of this issue is clearly demonstrated by ECCO, which provides accurate advective and diffusive transport terms computed online during model integration. Users relying solely on temperature–velocity output risk introducing substantial and spurious biases; producers of one degree resolution reanalyses are therefore strongly encouraged to provide online-computed diagnostics and to explicitly caution users against the UVT approach at this resolution.

https://doi.org/10.5194/egusphere-2026-5435
Preprint. Discussion started: 14 September 2026

The highest-resolution products (1/12) do not systematically outperform the lower-resolution systems (1/4 or 1 degree), suggesting that differences in model formulation, forcing and assimilation strategy can be as important as nominal horizontal resolution. The ensemble mean heat-budget-derived time mean MHT agrees closely with available observational estimates at most evaluated sections, supporting the usefulness of vertically integrated energy-budget methods as an additional benchmark for ocean reanalysis evaluation. This agreement is particularly encouraging given that the inferred estimates are largely independent of the ocean circulation fields used in the ocean reanalyses themselves. At the same time, the SAMBA comparison highlights an important limitation: inferred estimates exhibit substantially larger discrepancies with direct observations when integrating over regions with large OHT towards regions with smaller OHT.

The overall agreement across estimates for temporal variability is generally better than that of the mean transports, but depends strongly on region and timescale. RAPID and the Greenland–Scotland Ridge show the most robust agreement between ORAs and observations from seasonal to interannual timescales, whereas OSNAP appears to be the most challenging section, with weak agreement between observations, reanalyses and heat-budget inferred estimates on interannual timescales. The comparatively strong agreement at RAPID may partly reflect the relatively dense observational coverage of the subtropical North Atlantic, which provides stronger constraints on the assimilative reanalyses, although the influence of the observing network is not explicitly assessed here. More generally, ORAs and observational estimates agree better for seasonal heat transport variability than they do deseasonalized monthly and interannual fluctuations, likely because the seasonal forcing by surface heat fluxes and winds, including the associated Ekman transport, is well constrained in the reanalyses. The strong reduction in skill from seasonal to interannual timescales at sections such as SAMBA and OSNAP demonstrates that agreement in the mean state or seasonal cycle does not necessarily imply skill in representing longer-term variability.

Trend analyses indicate a broad reduction of northward Atlantic heat transport across the reanalysis ensemble since the early 1990s, although substantial uncertainties remain, particularly prior to the Argo era. At 26.5°N, the reanalysis ensemble trend over the RAPID period agrees in general with the observed RAPID decline, despite the fact that the transport observations are not directly assimilated by the reanalyses. This agreement provides some support for a recent reduction in subtropical Atlantic heat transport across independent observing and reanalysis systems, although the observational record remains too short to robustly establish a long-term trend. Nevertheless, the magnitude of long-term trends remains uncertain, particularly before the Argo and RAPID era, when subsurface observations were more limited and reanalysis products diverge more strongly. Heat-budget-derived estimates likewise generally show negative trends in northward heat transport, although the magnitude and statistical significance of the inferred trends depend on the applied energy-budget adjustment method and the choice of integration boundary. An alternative interpretation of the non-significance of many of the trend estimates is that the length of record is too short for long-term trends to emerge from variability. Nevertheless, all methodological choices considered here yield the same qualitative picture of negative MHT trends. At the RAPID latitude (26.5°N), the reanalysis ensemble indicates 1993–2023 trends of -0.058 ± 0.039 PW decade^{-1} in MHT and -1.23 ± 0.57 Sv decade^{-1} in AMOC strength. Excluding ORAS5 and CIGAR025, the two products with the strongest negative trends, reduces these estimates to -0.045 ± 0.037 PW decade^{-1} and -0.87 ± 0.54 Sv decade^{-1}, respectively, while both remain negative. Thus, while the magnitude of the estimated trends remains uncertain, their negative sign is consistent across the reanalysis ensemble considered here.

https://doi.org/10.5194/egusphere-2026-5435
Preprint. Discussion started: 14 September 2026

Our results extend the earlier ORA-IP assessment of Jackson et al. (2019) to a newer generation of reanalyses, a broader observational network and records extending into the early 2020s. The previously identified low bias at RAPID persists, while the present analysis additionally reveals strong regional and timescale dependence in reanalysis performance and shows that the highest-resolution products do not systematically outperform eddy-permitting systems. Extending the observational and reanalysis records remains important for distinguishing long-term changes from decadal variability, particularly given the larger uncertainties prior to Argo.

Taken together, these results demonstrate both the value and limitations of ORAs for studying Atlantic heat transport. Reanalyses provide a spatially complete and dynamically consistent view of ocean heat transport variability, but substantial differences remain in their representation of mean transports, unresolved eddy contributions and low-frequency variability, at key observing sections. Continued evaluation against sustained observations will be essential for improving confidence in reanalysis-based assessments of ocean heat transport and its role in climate variability and change. More broadly, this study demonstrates how application-oriented evaluation against independent benchmarks can provide practical guidance on the fitness-for-purpose of ORAs, thereby supporting their wider use in climate monitoring and future climate assessments.

Appendix: Supplemental figures

Appendix A1

https://doi.org/10.5194/egusphere-2026-5435
Preprint. Discussion started: 14 September 2026

Product	SAMBA [PW] 1993–	RAPID [PW] 2004–	OSNAP [PW] 2014–	GSR [PW] 1993–	Davis [TW] 2004–	Barents [TW] 2004–	Fram [TW] 2004–
GLORYS12V1 (1/12°)	0.45	0.95	0.52	0.24	5.1	81.3	35.3
SODAv4 (1/10°)	0.38	0.99	0.43	0.22	10.3	70.8	43.3
ORAS6-pilot (1/4°)	0.22	1.11	0.51	0.25	8.4	96.6	41.6
ORAS5 (1/4°)	0.30	0.95	0.48	0.22	13.4	80.0	32.7
CGLORSv8 (1/4°)	0.36	0.90	0.48	0.27	12.6	85.7	47.1
CGLORSv7 (1/4°)	0.42	1.12	0.45	0.26	5.1	77.6	40.5
GLORYS4V2 (1/4°)	0.48	1.06	0.46	0.24	7.7	84.2	36.7
GLORYS2V4 (1/4°)	0.50	0.96	0.46	0.23	2.2	85.1	23.8
GloSIA9-1 (1/4°)	0.20	0.88	0.43	0.24	4.4	78.9	37.3
GloRANV14 (1/4°)	0.33	0.93	0.45	0.25	9.3	87.5	42.9
SODAv3 (1/4°)	0.36	0.80	0.41	0.24	4.8	77.1	46.4
CIGAR0.25 (1/4°)	0.37	1.13	0.45	0.24	10.2	83.0	35.4
OCCA2 (1°)	0.34	0.81	0.39	0.26	7.6	110.0	18.5
ECCO4r6 (1°)	0.38	0.84	0.40	0.25	9.8	84.4	18.5
CIGAR (1°)	0.31	0.50	0.39	0.22	-4.0	70.8	13.5
ESTOCv7a (1°)	0.24	0.71	0.37	0.04	7.1	13.5	21.5
ESTOCv3a (1°)	0.35	0.81	0.35	0.04	-4.9	7.8	16.3
Inferred	0.41 ± 0.19	1.18 ± 0.09	0.45 ± 0.04	0.28 ± 0.03			
Observations	0.53 ± 0.21	1.21 ± 0.12	0.51 ± 0.09	0.28 ± 0.05	23.9 ± 11	64.8 ± 26	50.4 ± 19

Table A1. Mean meridional heat transport estimates from the ORAs, heat-budget-derived (inferred) estimates, and observational reference sections. Values are computed over the common observational periods indicated below the section names, or the maximum available overlap where shorter reanalysis records are used. Heat transports are reported in PW for SAMBA, RAPID, OSNAP, and the Greenland–Scotland Ridge (GSR), and in TW for Davis Strait, the Barents Sea Opening, and Fram Strait. ORAs are grouped according to their nominal horizontal resolution.

https://doi.org/10.5194/egusphere-2026-5435
Preprint. Discussion started: 14 September 2026

Product	Fram [Sv] 2004–	Barents [Sv] 2004–	Fram+Barents [Sv] 2004–
GLORYS12V1	-1.75	2.87	1.11
SODAv4	-1.82	2.64	0.82
ORAS6-pilot	-1.87	3.92	2.05
ORAS5	-1.73	3.42	1.69
CGLORSv8	-2.62	3.28	0.66
CGLORSv7	-2.09	3.08	0.99
GLORYS4V2	-2.75	2.91	0.15
GLORYS2V4	-2.63	3.37	0.74
GloSIA9-1	-2.58	3.06	0.48
GloRANV14	-3.25	3.48	0.23
SODAv3	-1.10	2.60	1.49
OCCA2	-3.82	4.15	0.32
ECCO4r6	-2.54	3.27	0.73
CIGAR	-2.01	2.96	0.95
ESTOCv3a	-0.99	0.31	-0.69
ESTOCv7a	-1.01	0.21	-0.82
Observations	-2.24 $\pm$ 0.77	2.61 $\pm$ 0.45	0.37 $\pm$ 0.89

Table A2. Mean volume transports through Fram Strait, the Barents Sea Opening and their sum over the common observational period. Positive values denote inflow to the Arctic Ocean and negative values denote outflow. ORAs are grouped according to their nominal horizontal resolution.

https://doi.org/10.5194/egusphere-2026-5435
Preprint. Discussion started: 14 September 2026

Ocean reanalysis	1993–	2004–
ORAS5	$-0.150 \pm 0.037^{*}$	$-0.062 \pm 0.059^{*}$
CIGAR025	$-0.122 \pm 0.043^{*}$	-0.020 ± 0.081
ORAS6-pilot	$-0.107 \pm 0.038^{*}$	$-0.085 \pm 0.067^{*}$
GloRANV14	$-0.075 \pm 0.048^{*}$	-0.004 ± 0.094
CGLORSv7	$-0.067 \pm 0.043^{*}$	$-0.095 \pm 0.082^{*}$
ESTOCv7a	$-0.057 \pm 0.032^{*}$	-0.001 ± 0.063
GloSIA9-1	$-0.056 \pm 0.048^{*}$	0.014 ± 0.088
CGLORSv8	$-0.038 \pm 0.036^{*}$	-0.020 ± 0.076
GLORYS2V4	-0.031 ± 0.032	-0.042 ± 0.063
GLORYS12V1	-0.030 ± 0.036	$-0.093 \pm 0.074^{*}$
SODA3	-0.028 ± 0.041	-0.015 ± 0.074
OCCA2	-0.025 ± 0.032	-0.007 ± 0.067
ECCO4r6	-0.015 ± 0.029	-0.002 ± 0.063
GLORYS4V2	-0.007 ± 0.039	0.010 ± 0.079
Ensemble mean	$-0.058 \pm 0.039^{*}$	-0.030 ± 0.052

Table A3. Linear trends in Atlantic meridional heat transport at 26.5°N over the 1993–2023 and 2004–2023 periods. Values are given as trend $\pm 2\,\mathrm{SE}_{\mathrm{AR1}}$ (PW decade^{-1}), where the trend standard error accounts for lag-1 autocorrelation in the regression residuals. Not all products span the full analysis periods; for each reanalysis, trends are calculated over the available record (see Tab. 1) within the respective period. The ensemble mean is reported as the mean reanalysis trend ± the combined uncertainty, including the inter-product spread and the autocorrelation-adjusted trend-estimation uncertainty. An asterisk (*) denotes a trend that is statistically significant ($p < 0.05$).

https://doi.org/10.5194/egusphere-2026-5435
Preprint. Discussion started: 14 September 2026

Adjustment	Atmospheric Reanalysis	Bering Strait	GSR/Davis
Global	ERA5	-0.013 ± 0.032	-0.015 ± 0.028
	JRA55	-0.020 ± 0.034	-0.023 ± 0.029
	JRA3Q	-0.015 ± 0.035	-0.022 ± 0.030
	MERRA2	-0.000 ± 0.035	-0.026 ± 0.030
Liu (2026)	ERA5	-0.018 ± 0.032	-0.018 ± 0.028
	JRA55	$-0.057 \pm 0.035^{*}$	$-0.045 \pm 0.028^{*}$
	MERRA2	-0.035 ± 0.036	$-0.056 \pm 0.030^{*}$
Ensemble mean		$-0.026 \pm 0.029/0.044$	

Table A4. Linear trends in inferred Atlantic meridional heat transport at 26.5°N for the different atmospheric forcing products, adjustment methods and integration boundaries over 1993–2023. Values are given as trend ± uncertainty (PW decade^{-1}). Individual estimates are reported as trend $\pm 2\,\mathrm{SE}_{\mathrm{AR1}}$, while the ensemble mean is reported using both the statistical trend uncertainty and the combined uncertainty shown in Fig. 10b. An asterisk (*) denotes trends that are statistically significant ($p < 0.05$).

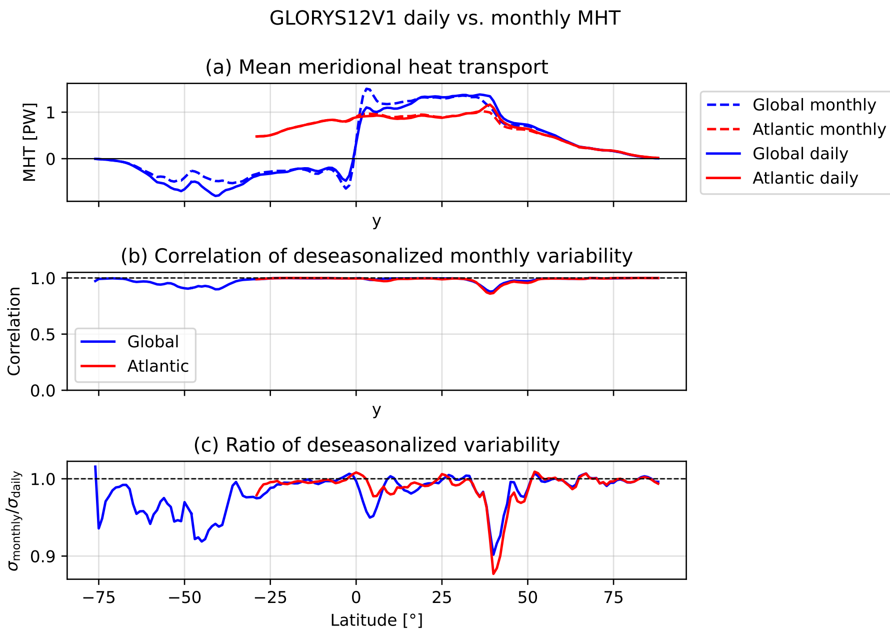

Figure A1. Comparison of meridional heat transport (MHT) calculated from daily and monthly GLORYS12V1 fields. (a) Mean global and Atlantic MHT calculated from daily (solid) and monthly (dashed) velocity and temperature fields. (b) Correlation between the deseasonalized monthly variability of the daily- and monthly-derived MHT. (c) Ratio of the standard deviation of deseasonalized monthly-derived to daily-derived MHT. The comparison illustrates the effect of neglecting sub-monthly velocity–temperature covariance terms when MHT is calculated from monthly mean fields.

https://doi.org/10.5194/egusphere-2026-5435
Preprint. Discussion started: 14 September 2026

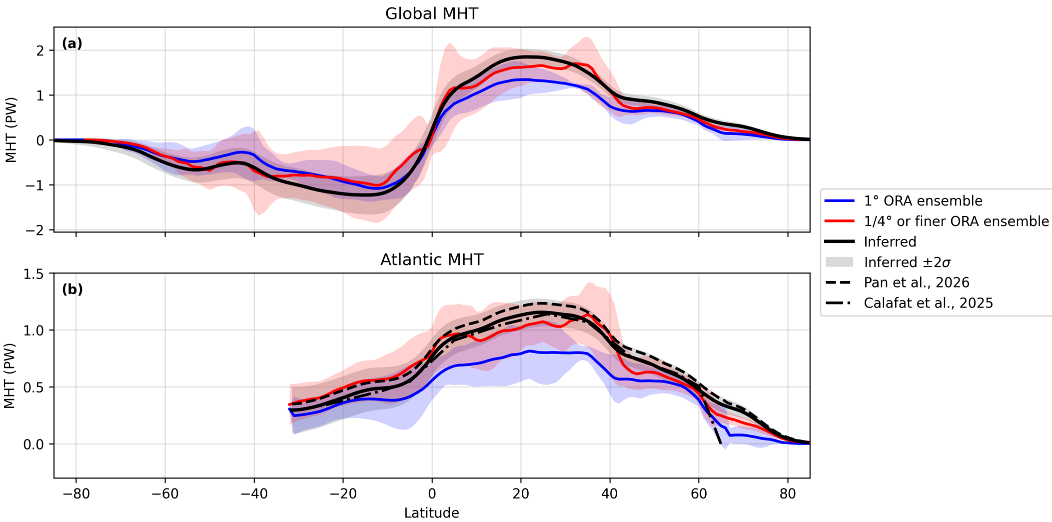

Figure A2. Mean meridional heat transport (MHT) as a function of latitude for the (a) global ocean and (b) Atlantic Ocean. ORAs are grouped into 1° products and products with a resolution of 1/4° or finer. Lines show the ensemble means and shaded envelopes indicate ±2 inter-product standard deviations. Mean transports are computed over the available period of each product (Table 1). The reanalysis ensembles are compared with heat-budget-derived estimates (black lines).

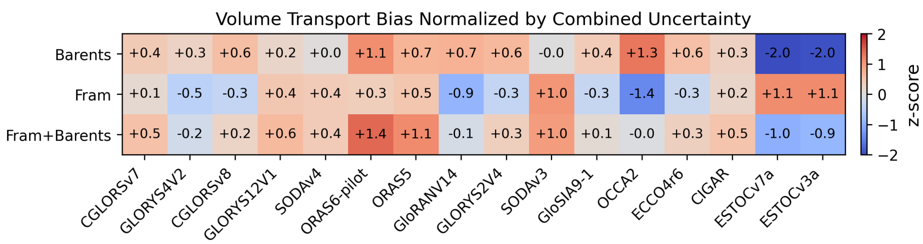

Figure A3. Mean volume transport biases through Fram Strait, the Barents Sea Opening, and their combined transport (Fram+Barents) expressed as standardized biases (z-scores). Biases are normalized by the combined observational uncertainty and inter-reanalysis spread. Positive values indicate larger (more positive) transports than observed, while negative values indicate smaller (more negative) transports than observed. For Fram Strait, where the observed transport is southward (negative), negative z-scores therefore correspond to a stronger-than-observed export.

https://doi.org/10.5194/egusphere-2026-5435
Preprint. Discussion started: 14 September 2026

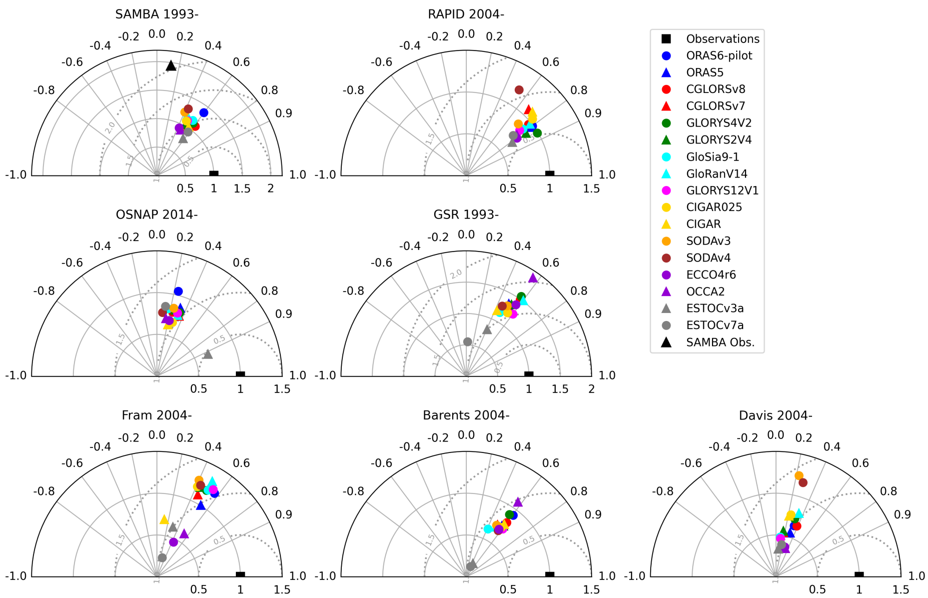

Figure A4. As in Figure 7, but for deseasonalized monthly heat transport anomalies without temporal smoothing. The mean seasonal cycle is removed separately for each product prior to computing Taylor statistics.

https://doi.org/10.5194/egusphere-2026-5435
Preprint. Discussion started: 14 September 2026

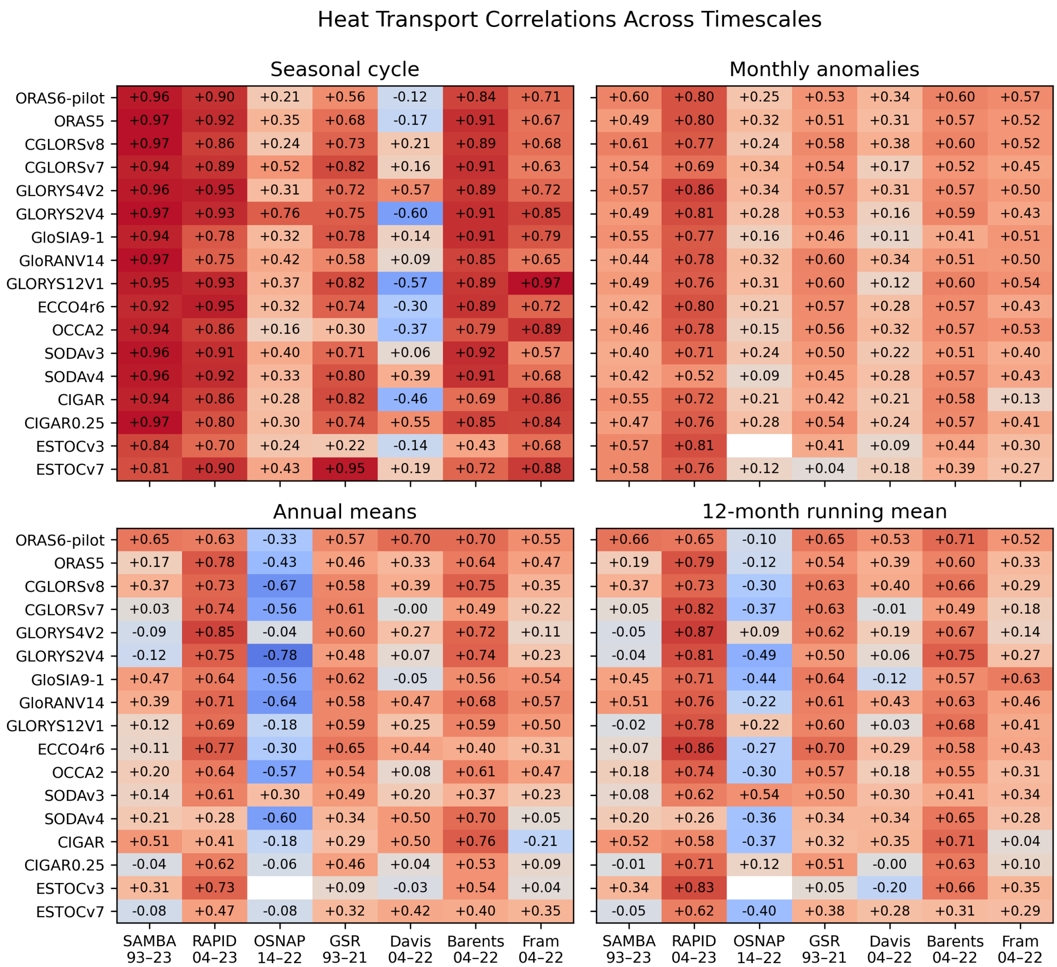

Figure A5. Correlations between observed and reanalysis-derived heat transports for different variability metrics. Panels show correlations of the seasonal cycle, deseasonalized monthly anomalies, annual-mean anomalies and 12-month running mean anomalies. Positive values indicate agreement in temporal variability, while values near zero or negative indicate weak or inconsistent agreement with observations.

https://doi.org/10.5194/egusphere-2026-5435
Preprint. Discussion started: 14 September 2026

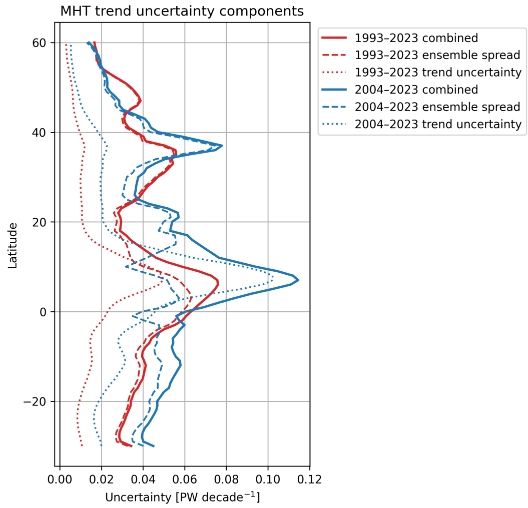

Figure A6. Decomposition of Atlantic MHT trend uncertainty. Ensemble-spread uncertainty (dashed), trend-estimation uncertainty derived from ordinary least-squares regression (dotted), and the resulting combined uncertainty (solid) for MHT trends computed over 1993–2023 (red) and 2004–2023 (blue). Combined uncertainty is calculated as the square root of the sum of squared ensemble-spread and trend-estimation uncertainties. Values represent 1σ uncertainties and are expressed in PW decade^{-1}.

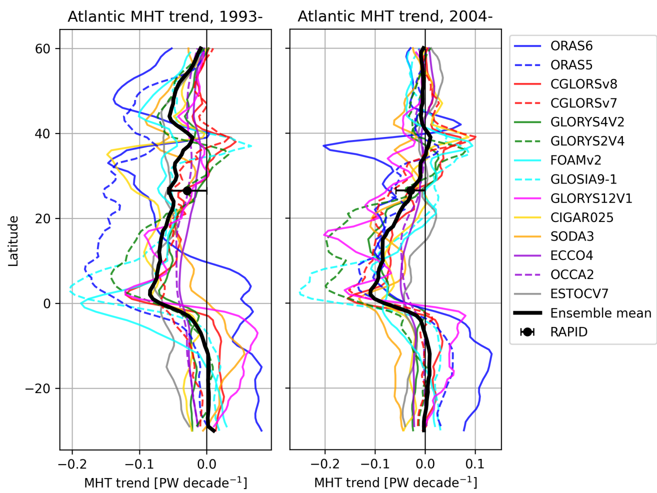

Figure A7. Atlantic meridional heat transport (MHT) trends from individual reanalysis products. Linear MHT trends as a function of latitude for individual ORAs over the periods 1993–2023 (left) and 2004–2023 (right). The thick black curve indicates the ensemble-mean trend. The black marker and horizontal error bar show the RAPID-derived MHT trend at 26.5°N for 2004–2023 ($\pm 1\sigma$).

https://doi.org/10.5194/egusphere-2026-5435
Preprint. Discussion started: 14 September 2026

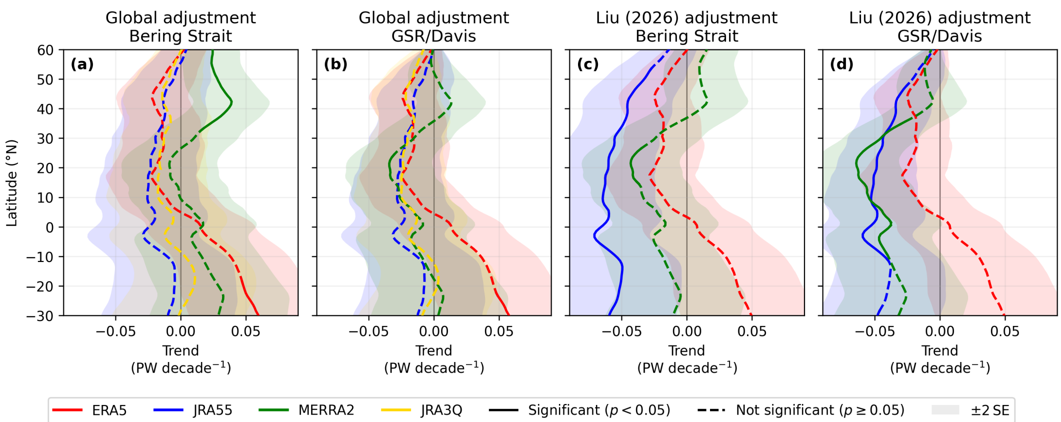

Figure A8. Linear trends in inferred Atlantic meridional heat transport (MHT) as a function of latitude for the different atmospheric forcing products and adjustment methods. Panels show estimates obtained using the global adjustment (a,b) and the adjustment of Liu (2026); Yang et al. (2026b) (c,d), with integration from the Bering Strait (left) and from the Greenland–Scotland Ridge/Davis Strait (right). Shading indicates the ± 2 standard error of the ordinary least-squares trend estimate. Solid line segments denote statistically significant trends ($p < 0.05$), whereas dashed segments indicate trends that are not statistically significant ($p \geq 0.05$).

https://doi.org/10.5194/egusphere-2026-5435
Preprint. Discussion started: 14 September 2026

Author contributions.

Acknowledgements. We thank Richard Renshaw for providing the GloSIA9-1 reanalysis data used in this study and for his helpful comments on the manuscript. S, Winkelbauer was supported by the Copernicus Marine Environment Service contract 24254L03-COP-GLORAN-MER IP-4000 and ESA Contract ref. 4000147586/I/25-LR (Ocean Surface Heat Flux). M. Mayer's efforts were supported by ESA contract ref. 4000145298/24/I-LR (MOTECUSOMA) and ESA Contract ref. 4000147586/I/25-LR (Ocean Surface Heat Flux). Open access funding provided by University of Vienna. ChatGPT (OpenAI) and DeepL were used to improve grammar and phrasing.

Code availability.

Data availability.

https://doi.org/10.5194/egusphere-2026-5435
Preprint. Discussion started: 14 September 2026

References

Bacon, S., Aksenov, Y., Fawcett, S., and Madec, G.: Arctic mass, freshwater and heat fluxes: methods and modelled seasonal variability, Philosophical Transactions of the Royal Society A: Mathematical, Physical and Engineering Sciences, 373, 20140 169, https://doi.org/10.1098/rsta.2014.0169, 2015.

Baker, J., Renshaw, R., Jackson, L., Dubois, C., Iovino, D., and Zuo, H.: Overturning variations in the subpolar North Atlantic in an ocean reanalyses ensemble, in: The Copernicus Marine Environment Monitoring Service Ocean State Report, Issue 6, edited by Le Traon, P. Y. et al., vol. 15, pp. S1–S142, https://doi.org/10.1080/1755876X.2022.2095169, 2022.

Baker, J. A., Renshaw, R., Jackson, L. C., Dubois, C., Iovino, D., Zuo, H., Perez, R. C., Dong, S., Kersalé, M., Mayer, M., Mayer, J., Speich, S., and Lamont, T.: South Atlantic overturning and heat transport variations in ocean reanalyses and observation-based estimates, State of the Planet, 1-osr7, 4, https://doi.org/10.5194/sp-1-osr7-4-2023, 2023.

Balmaseda, M., Hernandez, F., Storto, A., Palmer, M., Alves, O., Shi, L., Smith, G., Toyoda, T., Valdivieso, M., Barnier, B., Behringer, D., Boyer, T., Chang, Y.-S., Chepurin, G., Ferry, N., Forget, G., Fujii, Y., Good, S., Guinehut, S., Haines, K., Ishikawa, Y., Keeley, S., Köhl, A., Lee, T., Martin, M., Masina, S., Masuda, S., Meyssignac, B., Mogensen, K., Parent, L., Peterson, K., Tang, Y., Yin, Y., Vernieres, G., Wang, X., Waters, J., Wedd, R., Wang, O., Xue, Y., Chevallier, M., Lemieux, J.-F., Dupont, F., Kuragano, T., Kamachi, M., Awaji, T., Caltabiano, A., Wilmer-Becker, K., and Gaillard, F.: The Ocean Reanalyses Intercomparison Project (ORA-IP), Journal of Operational Oceanography, 8, s80–s97, https://doi.org/10.1080/1755876X.2015.1022329, 2015.

Baringer, M. O. and Garzoli, S. L.: Meridional heat transport determined with expendable bathythermographs—Part I: Error estimates from model and hydrographic data, Deep Sea Research Part I: Oceanographic Research Papers, 54, 1390–1401, https://doi.org/10.1016/j.dsr.2007.03.011, 2007.

Buckley, M. W. and Marshall, J.: Observations, inferences, and mechanisms of the Atlantic Meridional Overturning Circulation: A review, Reviews of Geophysics, 54, 5–63, https://doi.org/10.1002/2015RG000493, 2016.

Calafat, F. M., Vallivattathillam, P., and Frajka-Williams, E.: Estimates of Atlantic meridional heat transport from spatiotemporal fusion of Argo, altimetry, and gravimetry data, Ocean Science, 21, 2743–2762, https://doi.org/10.5194/os-21-2743-2025, 2025.

Carton, J. A., Chepurin, G. A., and Chen, L.: SODA3: A New Ocean Climate Reanalysis, Journal of Climate, 31, 6967 – 6983, https://doi.org/10.1175/JCLI-D-18-0149.1, 2018.

Cheng, L., Pan, Y., Tan, Z., Zheng, H., Zhu, Y., Wei, W., Du, J., Yuan, H., Li, G., Ye, H., Gouretski, V., Li, Y., Trenberth, K. E., Abraham, J., Jin, Y., Reseghetti, F., Lin, X., Zhang, B., Chen, G., Mann, M. E., and Zhu, J.: IAPv4 ocean temperature and ocean heat content gridded dataset, Earth System Science Data, 16, 3517–3546, https://doi.org/10.5194/essd-16-3517-2024, 2024.

Chepurin, G. A., Carton, J. A., Sun, L., and Penny, S. G.: SODA4: a mesoscale ocean/sea ice reanalysis 1980–2024, EGUsphere, 2025, 1–28, https://doi.org/10.5194/egusphere-2025-3810, 2025.

de Boisséson, E., Mayer, M., Winkelbauer, S., Tietsche, S., Pelletier, C., Balmaseda, M., Zuo, H., et al.: Evaluation of Climate Signals in the ECMWF Ocean Reanalysis ORAS6, in preparation, 2026.

Desportes, C., Garric, G., Régnier, C., Drévillon, M., Parent, L., Drillet, Y., Masina, S., Storto, A., Mirouze, I., Cipollone, A., Zuo, H., Balmaseda, M., Peterson, D., Wood, R., Jackson, L., Mulet, S., and Greiner, E.: Global Ocean Ensemble Physics Reanalysis, https://doi.org/10.48670/moi-00024, 2017.

Dong, S., Goni, G., Domingues, R., Bringas, F., Goes, M., Christophersen, J., and Baringer, M.: Synergy of In Situ and Satellite Ocean Observations in Determining Meridional Heat Transport in the Atlantic Ocean, Journal of Geophysical Research: Oceans, 126, e2020JC017 073, https://doi.org/10.1029/2020JC017073, 2021.

ECCO Consortium, Fukumori, I., Wang, O., Fenty, I., Forget, G., Heimbach, P., and Ponte, R. M.: Synopsis of the ECCO Central Production Global Ocean and Sea-Ice State Estimate (Version 4 Release 4), https://doi.org/10.5281/zenodo.4533349, 2021a.

ECCO Consortium, Fukumori, I., Wang, O., Fenty, I., Forget, G., Heimbach, P., and Ponte, R. M.: ECCO Central Estimate (Version 4 Release 4), https://ecco-group.org/products-ECCO-V4r4.htm, dataset, accessed 2025-11-01, 2021b.

Fasullo, J. T. and Trenberth, K. E.: The Annual Cycle of the Energy Budget. Part I: Global Mean and Land–Ocean Exchanges, Journal of Climate, 21, 2297 – 2312, https://doi.org/10.1175/2007JCLI1935.1, 2008.

Forget, G.: Mapping ocean observations in a dynamical framework: A 2004-06 ocean atlas, Journal of Physical Oceanography, 40, https://doi.org/10.1175/2009JPO4043.1, 2010.

Forget, G.: Ocean Heat Transport Convergence Drives Regional Energy Imbalance in the Sunlit Ocean Layer, EGUsphere, 2026, 1–38, https://doi.org/10.5194/egusphere-2026-4643, 2026.

Forget, G. and Ferreira, D.: Global ocean heat transport dominated by heat export from the tropical Pacific, Nature Geoscience, 12, 351–354, https://doi.org/10.1038/s41561-019-0333-7, 2019.

Forget, G., Ferron, B., and Mercier, H.: Combining Argo profiles with a general circulation model in the North Atlantic. Part 1: Estimation of hydrographic and circulation anomalies from synthetic profiles, over a year, Ocean Modelling, 20, 1–16, https://doi.org/10.1016/j.ocemod.2007.06.001, 2008a.

Forget, G., Mercier, H., and Ferron, B.: Combining Argo profiles with a general circulation model in the North Atlantic. Part 2: Realistic transports and improved hydrography, between spring 2002 and spring 2003, Ocean Modelling, 20, 17–34, https://doi.org/10.1016/j.ocemod.2007.06.002, 2008b.

Forget, G., Campin, J.-M., Heimbach, P., Hill, C. N., Ponte, R. M., and Wunsch, C.: ECCO Version 4: An Integrated Framework for Nonlinear Inverse Modeling and Global Ocean State Estimation, Geoscientific Model Development, 8, 3071–3104, https://doi.org/10.5194/gmd-8-3071-2015, 2015.

Fredriksen, H., de Steur, L., von Appen, W.-J., Ingvaldsen, R., McPherson, R., Lee, C., Lenetsky, J., and Woodgate, R.: Pan-Arctic Gateway transports since 2004, https://doi.org/10.21334/NPOLAR.2025.80B69907, 2025.

Fu, Y., Lozier, M. S., Bower, A., Burmeister, K., Carrilho Biló, T., Cyr, F., Cunningham, S. A., deYoung, B., Fehmi Dilmahamod, A., and de Jong, M. F.: Meridional Overturning Circulation Observed by the Overturning in the Subpolar North Atlantic Program (OSNAP) Array from August 2014 to July 2022, https://doi.org/10.35090/gatech/78023, dataset, 2025.

Garric, G. and L.Parent: GLobal Ocean ReanalYses and Simulations: GLORYS2V4 product Scientific and technical notice for users, https://www.mercator-ocean.eu/wp-content/uploads/2017/06/GLORYS2V4_technical_features_OCT2016.pdf, 2016.

Garzoli, S. L., Baringer, M. O., Dong, S., Perez, R. C., and Yao, Q.: South Atlantic meridional fluxes, Deep Sea Research Part I: Oceanographic Research Papers, 71, 21–32, https://doi.org/10.1016/j.dsr.2012.09.003, 2013.

Gelaro, R., McCarty, W., Suárez, M. J., Todling, R., Molod, A., Takacs, L., Randles, C. A., Darmenov, A., Bosilovich, M. G., Reichle, R., Wargan, K., Coy, L., Cullather, R., Draper, C., Akella, S., Buchard, V., Conaty, A., da Silva, A. M., Gu, W., Kim, G.-K., Koster, R., Lucchesi, R., Merkova, D., Nielsen, J. E., Partyka, G., Pawson, S., Putman, W., Rienecker, M., Schubert, S. D., Sienkiewicz, M., and Zhao, B.: The Modern-Era Retrospective Analysis for Research and Applications, Version 2 (MERRA-2), Journal of Climate, 30, 5419 – 5454, https://doi.org/10.1175/JCLI-D-16-0758.1, 2017.

Hersbach, H., Bell, B., Berrisford, P., Hirahara, S., Horányi, A., Muñoz-Sabater, J., Nicolas, J., Peubey, C., Radu, R., Schepers, D., Simmons, A., Soci, C., Abdalla, S., Abellan, X., Balsamo, G., Bechtold, P., Biavati, G., Bidlot, J., Bonavita, M., De Chiara, G., Dahlgren, P., Dee, D., Diamantakis, M., Dragani, R., Flemming, J., Forbes, R., Fuentes, M., Geer, A., Haimberger, L., Healy, S., Hogan, R. J., Hólm, E., Janisková, M., Keeley, S., Laloyaux, P., Lopez, P., Lupu, C., Radnoti, G., de Rosnay, P., Rozum, I., Vamborg, F., Villaume, S., and Thépaut, J.-N.: The ERA5 global reanalysis, Quarterly Journal of the Royal Meteorological Society, 146, 1999–2049, https://doi.org/10.1002/qj.3803, 2020.

Jackson, L. C., Dubois, C., Forget, G., Haines, K., Harrison, M., Iovino, D., Köhl, A., Mignac, D., Masina, S., Peterson, K. A., Piecuch, C. G., Roberts, C. D., Robson, J., Storto, A., Toyoda, T., Valdivieso, M., Wilson, C., Wang, Y., and Zuo, H.: The Mean State and Variability of the North Atlantic Circulation: A Perspective From Ocean Reanalyses, Journal of Geophysical Research: Oceans, 124, 9141–9170, https://doi.org/10.1029/2019JC015210, 2019.

Jean-Michel, L., Eric, G., Romain, B.-B., Gilles, G., Angélique, M., Marie, D., Clément, B., Mathieu, H., Olivier, L. G., Charly, R., Tony, C., Charles-Emmanuel, T., Florent, G., Giovanni, R., Mounir, B., Yann, D., and Pierre-Yves, L. T.: The Copernicus Global 1/12° Oceanic and Sea Ice GLORYS12 Reanalysis, Frontiers in Earth Science, Volume 9 - 2021, https://doi.org/10.3389/feart.2021.698876, 2021.

Johns, W. E., Baringer, M. O., Beal, L. M., Cunningham, S. A., Kanzow, T., Bryden, H. L., Hirschi, J. J. M., Marotzke, J., Meinen, C. S., Shaw, B., and Curry, R.: Continuous, Array-Based Estimates of Atlantic Ocean Heat Transport at 26.5°N, Journal of Climate, 24, 2429 – 2449, https://doi.org/10.1175/2010JCLI3997.1, 2011.

Johns, W. E., Elipot, S., Smeed, D. A., Moat, B., King, B., Volkov, D. L., and Smith, R. H.: Towards two decades of Atlantic Ocean mass and heat transports at 26.5° N, Philosophical Transactions of the Royal Society A: Mathematical, Physical and Engineering Sciences, 381, 20220 188, https://doi.org/10.1098/rsta.2022.0188, 2023.

Kersalé, M., Meinen, C. S., Perez, R. C., Hénaff, M. L., Valla, D., Lamont, T., Sato, O. T., Dong, S., Terre, T., van Caspel, M., Chidichimo, M. P., van den Berg, M., Speich, S., Piola, A. R., Campos, E. J. D., Ansorge, I., Volkov, D. L., Lumpkin, R., and Garzoli, S. L.: Highly variable upper and abyssal overturning cells in the South Atlantic, Science Advances, 6, eaba7573, https://doi.org/10.1126/sciadv.aba7573, 2020.

Kersalé, M., Meinen, C. S., Perez, R. C., Piola, A. R., Speich, S., Campos, E. J. D., Garzoli, S. L., Ansorge, I., Volkov, D. L., Le Hénaff, M., Dong, S., Lamont, T., Sato, O. T., and van den Berg, M.: Multi-Year Estimates of Daily Heat Transport by the Atlantic Meridional Overturning Circulation at 34.5°S, Journal of Geophysical Research: Oceans, 126, e2020JC016 947, https://doi.org/10.1029/2020JC016947, 2021.

Kobayashi, S., Ota, Y., Harada, Y., Ebita, A., Moriya, M., Onoda, H., Onogi, K., Kamahori, H., Kobayashi, C., Endo, H., Miyaoka, K., and Takahashi, K.: The JRA-55 Reanalysis: General Specifications and Basic Characteristics, Journal of the Meteorological Society of Japan. Ser. II, 93, 5–48, https://doi.org/10.2151/jmsj.2015-001, 2015.

KOSAKA, Y., KOBAYASHI, S., HARADA, Y., KOBAYASHI, C., NAOE, H., YOSHIMOTO, K., HARADA, M., GOTO, N., CHIBA, J., MIYAOKA, K., SEKIGUCHI, R., DEUSHI, M., KAMAHORI, H., NAKAEGAWA, T., TANAKA, T. Y., TOKUHIRO, T., SATO, Y., MATSUSHITA, Y., and ONOGI, K.: The JRA-3Q Reanalysis, Journal of the Meteorological Society of Japan. Ser. II, 102, 49–109, https://doi.org/10.2151/jmsj.2024-004, 2024.

Lellouche, J.-M., Greiner, E., Le Galloudec, O., Garric, G., Regnier, C., Drevillon, M., Benkiran, M., Testut, C.-E., Bourdalle-Badie, R., Gasparin, F., Hernandez, O., Levier, B., Drillet, Y., Remy, E., and Le Traon, P.-Y.: Recent updates to the Copernicus Marine Service global ocean monitoring and forecasting real-time $1/12°$ high-resolution system, Ocean Science, 14, 1093–1126, https://doi.org/10.5194/os-14-1093-2018, 2018.

Liu, C.: Energy balance data, https://doi.org/10.57760/sciencedb.32616, 2026.

Liu, C., Allan, R. P., Mayer, M., Hyder, P., Desbruyères, D., Cheng, L., Xu, J., Xu, F., and Zhang, Y.: Variability in the global energy budget and transports 1985–2017, Climate Dynamics, 55, 3381–3396, https://doi.org/10.1007/s00382-020-05451-8, 2020.

Loeb, N. G., Doelling, D. R., Wang, H., Su, W., Nguyen, C., Corbett, J. G., Liang, L., Mitrescu, C., Rose, F. G., and Kato, S.: Clouds and the Earth's Radiant Energy System (CERES) Energy Balanced and Filled (EBAF) Top-of-Atmosphere (TOA) Edition-4.0 Data Product, Journal of Climate, 31, 895 – 918, https://doi.org/10.1175/JCLI-D-17-0208.1, 2018.

Lozier, M. S., Bacon, S., Bower, A. S., Cunningham, S. A., de Jong, M. F., de Steur, L., deYoung, B., Fischer, J., Gary, S. F., Greenan, B. J. W., Heimbach, P., Holliday, N. P., Houpert, L., Inall, M. E., Johns, W. E., Johnson, H. L., Karstensen, J., Li, F., Lin, X., Mackay, N., Marshall, D. P., Mercier, H., Myers, P. G., Pickart, R. S., Pillar, H. R., Straneo, F., Thierry, V., Weller, R. A., Williams, R. G., Wilson, C., Yang, J., Zhao, J., and Zika, J. D.: Overturning in the Subpolar North Atlantic Program: A New International Ocean Observing System, Bulletin of the American Meteorological Society, 98, 737 – 752, https://doi.org/10.1175/BAMS-D-16-0057.1, 2017.

Lozier, M. S., Li, F., Bacon, S., Bahr, F., Bower, A. S., Cunningham, S. A., de Jong, M. F., de Steur, L., deYoung, B., Fischer, J., Gary, S. F., Greenan, B. J. W., Holliday, N. P., Houk, A., Houpert, L., Inall, M. E., Johns, W. E., Johnson, H. L., Johnson, C., Karstensen, J., Koman, G., Bras, I. A. L., Lin, X., Mackay, N., Marshall, D. P., Mercier, H., Oltmanns, M., Pickart, R. S., Ramsey, A. L., Rayner, D., Straneo, F., Thierry, V., Torres, D. J., Williams, R. G., Wilson, C., Yang, J., Yashayaev, I., and Zhao, J.: A sea change in our view of overturning in the subpolar North Atlantic, Science, 363, 516–521, https://doi.org/10.1126/science.aau6592, 2019.

Lyman, J. M. and Johnson, G. C.: Global High-Resolution Random Forest Regression Maps of Ocean Heat Content Anomalies Using In Situ and Satellite Data, Journal of Atmospheric and Oceanic Technology, 40, 575 – 586, https://doi.org/10.1175/JTECH-D-22-0058.1, 2023.

MacLachlan, C., Arribas, A., Peterson, K. A., Maidens, A., Fereday, D., Scaife, A. A., Gordon, M., Vellinga, M., Williams, A., Comer, R. E., Camp, J., Xavier, P., and Madec, G.: Global Seasonal forecast system version 5 (GloSea5): a high-resolution seasonal forecast system, Quarterly Journal of the Royal Meteorological Society, 141, 1072–1084, https://doi.org/10.1002/qj.2396, 2015.

Mayer, J., Haimberger, L., and Mayer, M.: A quantitative assessment of air–sea heat flux trends from ERA5 since 1950 in the North Atlantic basin, Earth System Dynamics, 14, 1085–1105, https://doi.org/10.5194/esd-14-1085-2023, 2023a.

Mayer, M., Tsubouchi, T., von Schuckmann, K., Seitner, V., Winkelbauer, S., and Haimberger, L.: Atmospheric and oceanic contributions to observed Nordic Seas and Arctic Ocean heat content variations 1993–2020, Journal of Operational Oceanography, 15, S20–S28, https://doi.org/10.1080/1755876X.2022.2095169, in: Copernicus Ocean State Report, Issue 6, 2022.

Mayer, M., Tsubouchi, T., Winkelbauer, S., Larsen, K. M. H., Berx, B., Macrander, A., Iovino, D., Jónsson, S., and Renshaw, R.: Recent variations in oceanic transports across the Greenland–Scotland Ridge, State of the Planet, 1-osr7, 14, https://doi.org/10.5194/sp-1-osr7-14-2023, 2023b.

Mayer, M., Kato, S., Bosilovich, M., Bechtold, P., Mayer, J., Schröder, M., Behrangi, A., Wild, M., Kobayashi, S., Li, Z., and L'Ecuyer, T.: Assessment of Atmospheric and Surface Energy Budgets Using Observation-Based Data Products, Surveys in Geophysics, 45, 1827–1854, https://doi.org/10.1007/s10712-024-09827-x, 2024.

McCarthy, G., Smeed, D., Johns, W., Frajka-Williams, E., Moat, B., Rayner, D., Baringer, M., Meinen, C., Collins, J., and Bryden, H.: Measuring the Atlantic Meridional Overturning Circulation at 26°N, Progress in Oceanography, 130, 91–111, https://doi.org/10.1016/j.pocean.2014.10.006, 2015.

McCarthy, G. D., Brown, P. J., Flagg, C. N., Goni, G., Houpert, L., Hughes, C. W., Hummels, R., Inall, M., Jochumsen, K., Larsen, K. M. H., Lherminier, P., Meinen, C. S., Moat, B. I., Rayner, D., Rhein, M., Roessler, A., Schmid, C., and Smeed, D. A.: Sustainable Observations

https://doi.org/10.5194/egusphere-2026-5435
Preprint. Discussion started: 14 September 2026

of the AMOC: Methodology and Technology, Reviews of Geophysics, 58, e2019RG000 654, https://doi.org/10.1029/2019RG000654, e2019RG000654 2019RG000654, 2020.

Meyssignac, B., Fourest, S., Mayer, M., Johnson, G. C., Calafat, F. M., Ablain, M., Boyer, T., Cheng, L., Desbruyères, D., Forget, G., Giglio, D., Kuusela, M., Locarnini, R., Lyman, J. M., Llovel, W., Mishonov, A., Reagan, J., Rousseau, V., and Benveniste, J.: North Atlantic Heat Transport Convergence Derived from a Regional Energy Budget Using Different Ocean Heat Content Estimates, Surveys in Geophysics, 45, 1855–1874, https://doi.org/10.1007/s10712-024-09865-5, 2024.

Moat, B. I., Smeed, D. A., Rayner, D., Johns, W. E., Smith, R., Volkov, D., Elipot, S., Petit, T., Kajtar, J., Baringer, M. O., and Collins, J.: Atlantic meridional overturning circulation observed by the RAPID-MOCHA-WBTS (RAPID-Meridional Overturning Circulation and Heatflux Array-Western Boundary Time Series) array at 26N from 2004 to 2024, https://doi.org/10.5285/48d0bf43-0598-ceb2-e063-7086abc062f1, 2026.

Osafune, S., Doi, T., Masuda, S., Sugiura, N., and Hemmi, T.: Estimated State of Ocean for Climate Research (ESTOC), https://doi.org/10.17596/0000106, data set, accessed YYYY-MM-DD, 2014.

Osafune, S., Masuda, S., Sugiura, N., and Doi, T.: Evaluation of the applicability of the Estimated State of the Global Ocean for Climate Research (ESTOC) data set, Geophysical Research Letters, 42, 4903–4911, https://doi.org/10.1002/2015GL063877, 2015.

Osafune, S., Kouketsu, S., Doi, T., Sugiura, N., and Masuda, S.: A global ocean state estimation using tidally induced vertical-mixing schemes, Ocean Modelling, 179, 102 111, https://doi.org/10.1016/j.ocemod.2022.102111, 2022.

Pan, Y., Cheng, L., Storto, A., Mayer, M., Gulev, S., Li, Y., Lyu, K., Zheng, H., and Yuan, H.: Ocean Meridional Heat Transport Estimated from Energy Budget Constraint, Journal of Climate, 39, 3001 – 3019, https://doi.org/10.1175/JCLI-D-25-0522.1, 2026.

Santer, B. D., Wigley, T. M. L., Boyle, J. S., Gaffen, D. J., Hnilo, J. J., Nychka, D., Parker, D. E., and Taylor, K. E.: Statistical significance of trends and trend differences in layer-average atmospheric temperature time series, Journal of Geophysical Research: Atmospheres, 105, 7337–7356, https://doi.org/10.1029/1999JD901105, 2000.

Schauer, U. and Beszczynska-Möller, A.: Problems with estimation and interpretation of oceanic heat transport – conceptual remarks for the case of Fram Strait in the Arctic Ocean, Ocean Science, 5, 487–494, https://doi.org/10.5194/os-5-487-2009, 2009.

Sinha, B., Smeed, D., McCarthy, G., Moat, B., Josey, S., Hirschi, J.-M., Frajka-Williams, E., Blaker, A., Rayner, D., and Madec, G.: The accuracy of estimates of the overturning circulation from basin-wide mooring arrays, Progress in Oceanography, 160, 101–123, https://doi.org/10.1016/j.pocean.2017.12.001, 2018.

Stepanov, V. N., Iovino, D., Masina, S., Storto, A., and Cipollone, A.: Methods of calculation of the Atlantic meridional heat and volume transports from ocean models at 26.5°N, Journal of Geophysical Research: Oceans, 121, 1459–1475, https://doi.org/10.1002/2015JC011007, 2016.

Storto, A. and Masina, S.: C-GLORSv5: an improved multipurpose global ocean eddy-permitting physical reanalysis, Earth System Science Data, 8, 679–696, https://doi.org/10.5194/essd-8-679-2016, 2016.

Storto, A. and Yang, C.: Acceleration of the ocean warming from 1961 to 2022 unveiled by large-ensemble reanalyses, Nature Communications, 15, 545, https://doi.org/10.1038/s41467-024-44749-7, 2024.

Storto, A., Masina, S., Simoncelli, S., Iovino, D., Cipollone, A., Drevillon, M., Drillet, Y., Schuckmann, K., Parent, L., Garric, G., Greiner, E., Desportes, C., Zuo, H., Balmaseda, M., and Peterson, K.: The added value of the multi-system spread information for ocean heat content and steric sea level investigations in the CMEMS GREP ensemble reanalysis product, Climate Dynamics, 53, https://doi.org/10.1007/s00382-018-4585-5, 2019.

https://doi.org/10.5194/egusphere-2026-5435
Preprint. Discussion started: 14 September 2026

Terhaar, J., Vogt, L., and Foukal, N. P.: Atlantic overturning inferred from air-sea heat fluxes indicates no decline since the 1960s, Nature Communications, 16, 222, https://doi.org/10.1038/s41467-024-55297-5, 2025.

Tietsche, S., Balmaseda, M., Zuo, H., Roberts, C., Mayer, M., and Ferranti, L.: The importance of North Atlantic Ocean transports for seasonal forecasts, Climate Dynamics, 55, 1995–2011, https://doi.org/10.1007/s00382-020-05364-6, 2020.

Trenberth, K. E. and Caron, J. M.: Estimates of Meridional Atmosphere and Ocean Heat Transports, Journal of Climate, 14, 3433 – 3443, https://doi.org/10.1175/1520-0442(2001)014<3433:EOMAAO>2.0.CO;2, 2001.

Trenberth, K. E. and Fasullo, J. T.: Atlantic meridional heat transports computed from balancing Earth's energy locally, Geophysical Research Letters, 44, 1919–1927, https://doi.org/10.1002/2016GL072475, 2017.

Trenberth, K. E., Zhang, Y., Fasullo, J. T., and Cheng, L.: Observation-Based Estimates of Global and Basin Ocean Meridional Heat Transport Time Series, Journal of Climate, 32, 4567 – 4583, https://doi.org/10.1175/JCLI-D-18-0872.1, 2019.

Tsubouchi, T., Våge, K., Hansen, B., Larsen, K. M. H., Østerhus, S., Johnson, C., Jónsson, S., and Valdimarsson, H.: Increased ocean heat transport into the Nordic Seas and Arctic Ocean over the period 1993–2016, Nature Climate Change, 11, 21–26, https://doi.org/10.1038/s41558-020-00941-3, 2021.

Tsubouchi, T., von Appen, W.-J., Kanzow, T., and de Steur, L.: Temporal Variability of the Overturning Circulation in the Arctic Ocean and the Associated Heat and Freshwater Transports during 2004–10, Journal of Physical Oceanography, 54, 81 – 94, https://doi.org/10.1175/JPO-D-23-0056.1, 2024.

UNESCO Ocean Decade: Marine Environment Reanalyses Evaluation Project (MER-EP), https://oceandecade.org/actions/marine-environment-reanalyses-evaluation-project/, accessed: 21 August 2025, 2025.

Uotila, P., Goosse, H., Haines, K., Chevallier, M., Barthélemy, A., Bricaud, C., Carton, J., Fučkar, N., Garric, G., Iovino, D., Kauker, F., Korhonen, M., Lien, V. S., Marnela, M., Massonnet, F., Mignac, D., Peterson, K. A., Sadikni, R., Shi, L., Tietsche, S., Toyoda, T., Xie, J., and Zhang, Z.: An assessment of ten ocean reanalyses in the polar regions, Climate Dynamics, 52, 1613–1650, https://doi.org/10.1007/s00382-018-4242-z, 2019.

Valdivieso, M., Haines, K., Zuo, H., and Lea, D.: Freshwater and heat transports from global ocean synthesis, Journal of Geophysical Research: Oceans, 119, 394–409, https://doi.org/10.1002/2013JC009357, 2014.

Volkov, D. L., Smith, R. H., Garcia, R. F., Smeed, D. A., Moat, B. I., Johns, W. E., and Baringer, M. O.: Florida Current transport observations reveal four decades of steady state, Nature Communications, 15, 7780, https://doi.org/10.1038/s41467-024-51879-5, 2024.

Winkelbauer, S., Mayer, M., Seitner, V., Zsoter, E., Zuo, H., and Haimberger, L.: Diagnostic evaluation of river discharge into the Arctic Ocean and its impact on oceanic volume transports, Hydrology and Earth System Sciences, 26, 279–304, https://doi.org/10.5194/hess-26-279-2022, 2022.

Winkelbauer, S., Mayer, M., and Haimberger, L.: StraitFlux – precise computations of water strait fluxes on various modeling grids, Geoscientific Model Development, 17, 4603–4620, https://doi.org/10.5194/gmd-17-4603-2024, 2024a.

Winkelbauer, S., Mayer, M., and Haimberger, L.: Validation of key Arctic energy and water budget components in CMIP6, Climate Dynamics, 62, 3891–3926, https://doi.org/10.1007/s00382-024-07105-5, 2024b.

Winkelbauer, S., Winterer, I., Mayer, M., Fu, Y., and Haimberger, L.: Subpolar Atlantic meridional heat transports from OSNAP and ocean reanalyses – a comparison, Ocean Science, 22, 629–651, https://doi.org/10.5194/os-22-629-2026, 2026.

Yang, C., Bourdallé-Badie, R., Drévillon, M., Araujo, J., Balmaseda, M., de Boisséson, E., Carton, J., Cheng, L., Cheng, S., Cipollone, A., Cocetta, F., Danabasoglu, G., Delhasse, A., Di Biagio, V., Forget, G., Fujii, Y., Haines, K., Iovino, D., Massonnet, F., Martin, M., Mauriello, P., Mayer, M., McAdam, R., Oke, P., Oikonomou, C. L. G., Ohishi, S., Osafune, S., Papasarafianou, S., De Rovere, F., Renshaw,

https://doi.org/10.5194/egusphere-2026-5435
Preprint. Discussion started: 14 September 2026

R., Smith, G. C., Selivanova, J., Storto, A., de Toma, V., Wen, C., Winkelbauer, S., Xie, J., and Zhang, H.: A user-oriented framework for evaluating ocean reanalyses: Ocean Decade action MER-EP (Marine Environment Reanalyses Evaluation Project), Bulletin of the American Meteorological Society, submitted, 2026a.

Yang, K., Liu, C., Li, J., Cao, N., Allan, R. P., and Mayer, M.: Update of the radiation fluxes at the top of atmosphere and net surface energy flux: DEEPC v5.1, https://doi.org/10.57760/sciencedb.28002, 2026b.

Zhang, J. and Rothrock, D. A.: Modeling Global Sea Ice with a Thickness and Enthalpy Distribution Model in Generalized Curvilinear Coordinates, Monthly Weather Review, 131, 845 – 861, https://doi.org/10.1175/1520-0493(2003)131<0845:MGSIWA>2.0.CO;2, 2003.

Zuo, H., Balmaseda, M. A., Tietsche, S., Mogensen, K., and Mayer, M.: The ECMWF operational ensemble reanalysis–analysis system for ocean and sea ice: a description of the system and assessment, Ocean Science, 15, 779–808, https://doi.org/10.5194/os-15-779-2019, 2019.